Delft University of Technology
Department of Aerospace Engineering
Delft

Prins Maurits Laboratory
Organization for Applied
Scientific Research TNO
Rijswijk

Report LR - 479
Report PML-1985 - C74
SFCC PUBLICATION NO. 31

VISIBLE RADIATION MEASUREMENT FOR TEMPERATURE DETERMINATION

P.J.M. Elands
T. Wijchers

Delft/Rijswijk, The Netherlands

November 1985

Delft University of Technology
Department of Aerospace Engineering
Delft

Prins Maurits Laboratory
Organization for Applied
Scientific Research TNO
Rijswijk

Report LR - 479
Report PML-1985 - C74
SFCC PUBLICATION NO. 31

VISIBLE RADIATION MEASUREMENT FOR TEMPERATURE DETERMINATION

P.J.M. Elands
T. Wijchers

Delft/Rijswijk, The Netherlands

November 1985

CONTENTS

SUMMARY

In this report, a method of temperature determination by measuring the visible radiation is described.
The theory of radiation according to the laws of Planck and Stefan-Boltzmann is treated, and also the detection of radiation and the detection geometrics are discussed.
The detector, consisting of a camera, a diode and an amplifier, was examined in order to determine all sorts of geometrics as, for example, lens openings, focal distance and principal planes. In this way, saturation and the error in adjustment were determined. The procedure of detector calibration by means of a tungsten ribbon lamp is described.
Measurements with the equipment to check the calibration constant were carried out on a piece of iron with known temperature.
A fairly good agreement was found between the results of this pyrometer method and temperature measurements with a thermocouple.

This project is sponsored by the Technology Foundation (Stichting voor de Technische Wetenschappen) and the Management Office for Energy Research PEO (Stichting Projektbeheerbureau Energie-Onderzoek).
In addition, means and manpower are made available by a special funding from Delft University of Technology (Beleidsruimte), while also manpower and computer facilities are provided by the Department of Aerospace Engineering, Delft University of Technology and the Prins Maurits Laboratory TNO.
This latter laboratory also provides the project with funding.

NOMENCLATURE

A	area
B	radiance
C	constant
d	diameter, distance
E	energy, output voltage
f	focal distance
F	focus
i	electric current
I	intensity, electric current
k	absorption per unit of length
l	length
n	refractive index
p	length
$\bar{p}$	location vector
P	power
$\bar{q}$	location vector
r	radius, length
R	resistor
s	pathlength, thickness
T	temperature
U	voltage
α	absorptivity
Δ	diaphragm number, difference
ε	emission factor or emissivity
λ	wavelength
ρ	reflectivity
σ	Stefan-Boltzmann constant
τ	transmittivity
Ω	solid angle

Indices

a	air
b	blackbody, bulk
BG	background
c	calibration/calibrated
d	detector

D	detectable
eff	effective
I	indicated
l	lens
m	measured
p	plexiglas
r	radiance, reflective
s	(radiating) surface, saturation
TRUE	true
λ	spectral

1. INTRODUCTION

At the Prins Maurits Laboratory TNO and at the Department of Aerospace Engineering of the Delft University of Technology, research is being carried out on Solid Fuel Combustion Chambers (SFCC's) (ref. 1). With solid fuel combustion, high temperatures, up to 3500 K can be achieved. As a consequence of such high temperatures, and also of the weathering by a chemically active environment, direct temperature measurement methods, for example with thermocouples, are not feasible. For that reason, use was made of an optical method of temperature determination, called pyrometry, as a simple substitute of a more elaborate spectrographic temperature determination.

Pyrometry is based on the relationship between absolute temperature and radiative power emitted by a medium. The intensity of radiation was measured with the aid of a detector. This dectector, together with an amplifier, was calibrated against a tungsten lamp of which the spectral intensity as well as the temperature, were known as a function of the applied electric current.

Since the radiation has to traverse the plexiglas wall of the combustion chamber, the decrease of light intensity due to reflection and absorption in plexiglas has to be taken into account. With help of the results of these calibrations, the flame temperature can be determined in a solid fuel combustion chamber. Because certain assumptions are involved in the determination of the temperatures, some systematic errors occur. However, when the errors are determined by comparing the results obtained with those obtained by spectrometry, pyrometry is considered to be a valuable tool for the SFCC project. Appendix C is a manual where the use of the detector, amplifier and additional screens are described (in Dutch).

2. THEORETICAL BACKGROUND

2.1. Radiation intensity and temperature

For blackbody radiation in vacuum, Planck found that the radiation spectral intensity per unit of area $I_{b\lambda}[W/m^3]$ is a function of the wavelength $\lambda[m]$ and the absolute temperature T:

$$I_{b\lambda} = \frac{2\,C_1}{\lambda^5\left(e^{C_2/\lambda T} - 1\right)} \qquad \text{(ref. 2)} \qquad (2.1)$$

where: $C_1 = 0.59548.10^{-16}$ Wm^2

$C_2 = 0.0143879$ mK

In figure 2.1 this relation is shown.

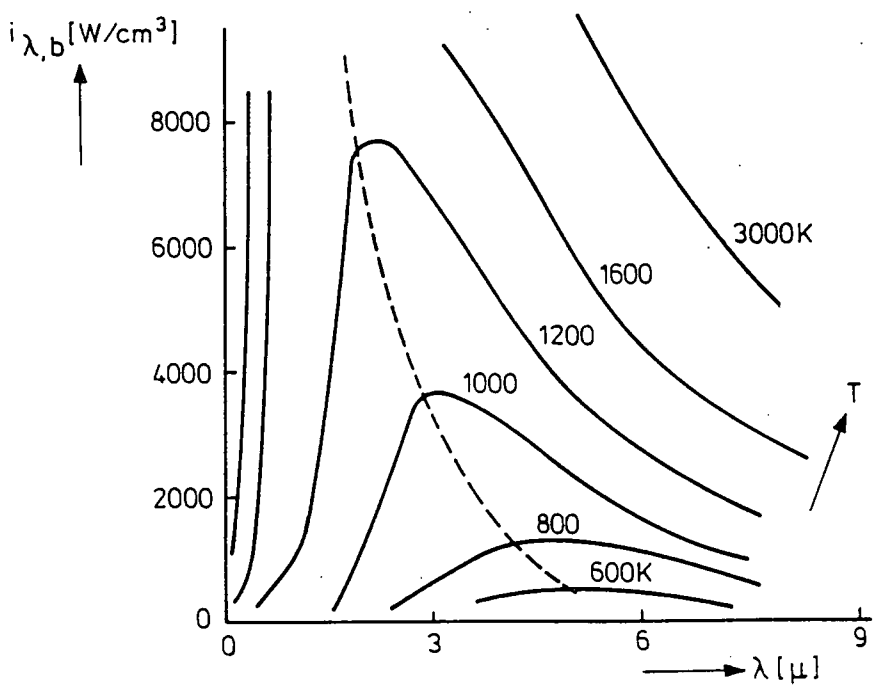

Fig. 2.1: Spectral intensity of blackbody radiation as a function of the wavelength.

The integrated spectral intensity, from now called intensity, in the wavelength range $\lambda_1 - \lambda_2$ is generally defined by:

$$I_{\lambda_1,\lambda_2} = \int_{\lambda_1}^{\lambda_2} I_\lambda \, d\lambda = \int_{o}^{\lambda_2} I_\lambda \, d\lambda - \int_{o}^{\lambda_1} I_\lambda \, d\lambda \qquad (2.2)$$

The dimension of I_{λ_1,λ_2} is power per unit area. For each temperature of a blackbody $I_{b,\lambda_1,\lambda_2}$ will have a different value, so the intensity in the wavelength range $\lambda_1 - \lambda_2$ may be a measure of the temperature. The temperature T can be derived from the radiation intensity by integrating (2.1) over the total wavelength range. It is assumed that $e^{C_2/\lambda T} - 1 = e^{C_2/\lambda T}$, where the integration of 2.1 is practically equal to the integration over the total wavelength range. The radiation intensity from a radiating surface in the <u>total</u> wavelength range is given by

$$I = \sigma.\varepsilon.T^4 \qquad \text{(ref. 2)} \qquad (2.3)$$

where σ is the Stefan-Boltzmann constant being $5.6703.10^{-8}$ $Wm^{-2}K^{-4}$ and ε is the mean spectral value for the emission factor.
For a blackbody, $\varepsilon = 1$, for other radiating surfaces, $o<\varepsilon<1$. The temperature, derived by measuring the radiation intensity, is the radiance temperature T_r. Only for a blackbody this temperature equals the true temperature T, while for other surfaces $T_r = T\,\varepsilon^{\frac{1}{4}}$ is consequently lower than T. With the detector used, a different relationship between T_r and T will be found, since this detector is only uniformly sensitive between 450 and 950 nm. However still T_r derived from measurement with the detector will be smaller than T.

2.2. Detection geometrics and sensitivity

The detector to be used, measures irradiant power in a certain wavelength range $\lambda_1 - \lambda_2$. This power P_{λ_1,λ_2}, entering the detector, is defined by:

$$P_{\lambda_1,\lambda_2} = B_{\lambda_1,\lambda_2} A_d \Omega_s \qquad (2.4)$$

where: B_{λ_1,λ_2} is the radiance of the radiating surface,
A_d is the sensitive area of the detector, perpendicular to the incident rays,
Ω_s is the mean solid angle of the radiating surface with respect to the detector and is defined by:

$$\Omega_s = \frac{A_s}{r^2} \tag{2.5}$$

where: A_s is the projected area of the radiating surface, perpendicular to the optical path between surface and detector,
r is the distance between the radiating surface and the centre of the detector.

From (2.4) and (2.5) follows:

$$P_{\lambda_1,\lambda_2} = B_{\lambda_1,\lambda_2} \frac{A_d A_s}{r^2} \tag{2.6}$$

The radiance B_{λ_1,λ_2} of a surface can easily be derived from the intensity per unit of area I_{λ_1,λ_2} by:

$$B_{\lambda_1,\lambda_2} = \frac{1}{\pi} I_{\lambda_1,\lambda_2} \qquad \text{(ref. 2)} \tag{2.7}$$

The detector to be used has a constant spectral sensitivity between λ_1 = 450 nm and λ_2 = 950 nm and is practically insensitive outside that wavelength region. Therefore the output signal E_{λ_1,λ_2} of this detector will be:

$$E_{\lambda_1,\lambda_2} = C \cdot B_{\lambda_1,\lambda_2} \frac{A_d A_s}{r^2} \tag{2.8}$$

The detector will be calibrated at standard values $B_{c,\lambda_1,\lambda_2}$, $A_{c,d}$, $A_{c,s}$ and r_c of B_{λ_1,λ_2}, A_d, A_s and r respectively according to:

$$E_{c,\lambda_1,\lambda_2} = C\, B_{c,\lambda_1,\lambda_2} \frac{A_{c,d} A_{c,s}}{r_c^2} \tag{2.9}$$

From (2.9) follows:

$$C = \frac{E_{c,\lambda_1,\lambda_2}\, r_c^2}{B_{c,\lambda_1,\lambda_2} \cdot A_{c,d} \cdot A_{c,s}} \tag{2.10}$$

To describe different experimental situations, it is useful to define the detectable area $A_D(r) = \Omega_d.r^2$ where Ω_d is the solid angle of acceptance of the detector, see figure 2.2.

Now there are three situations (see figure 2.3):

1. The whole detectable area is covered by the radiating surface: $A_{eff} = A_D(r)$.
2. The whole radiating surface is covered by the detectable area: $A_{eff} = A_s$, this situation will occur mostly.
3. Part of the radiating surface is covered by part of the detectable area.

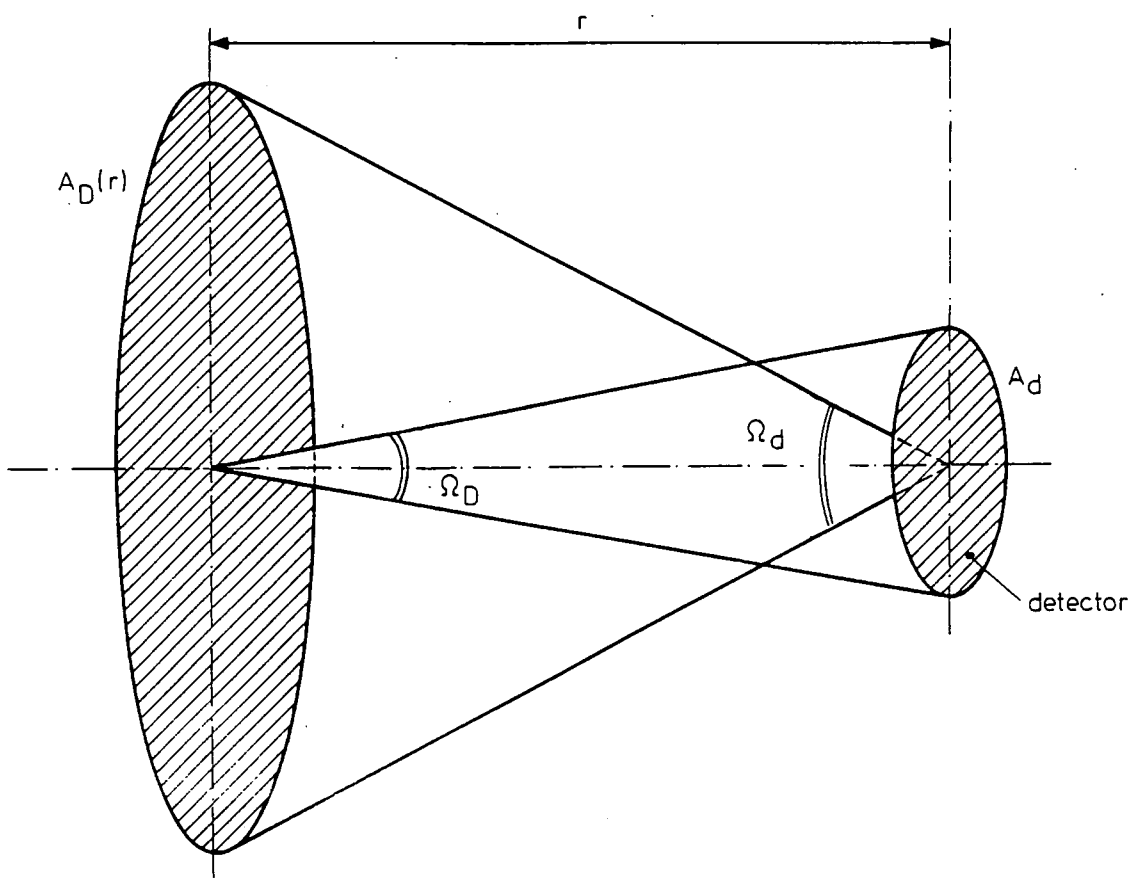

Figure 2.2: Detection geometrics.

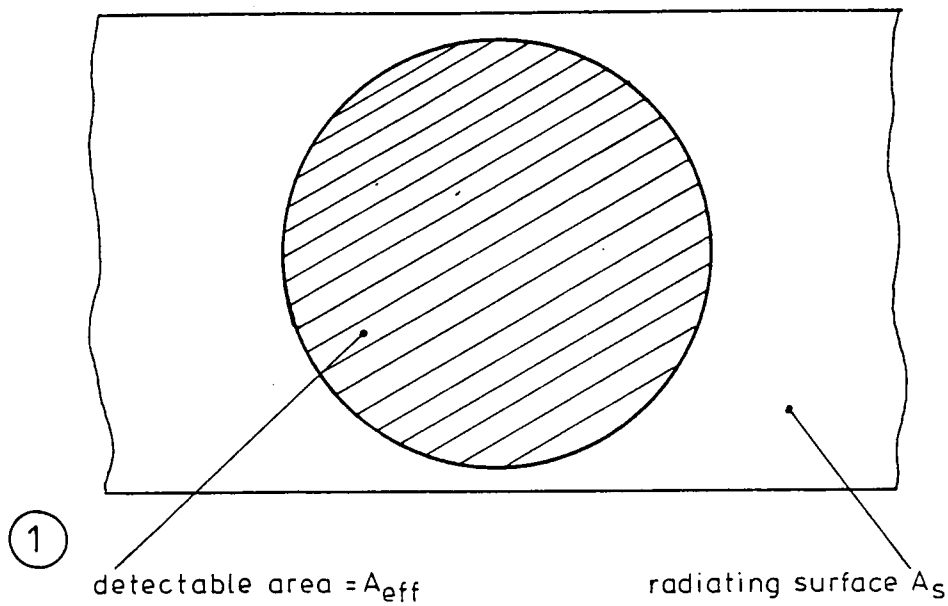

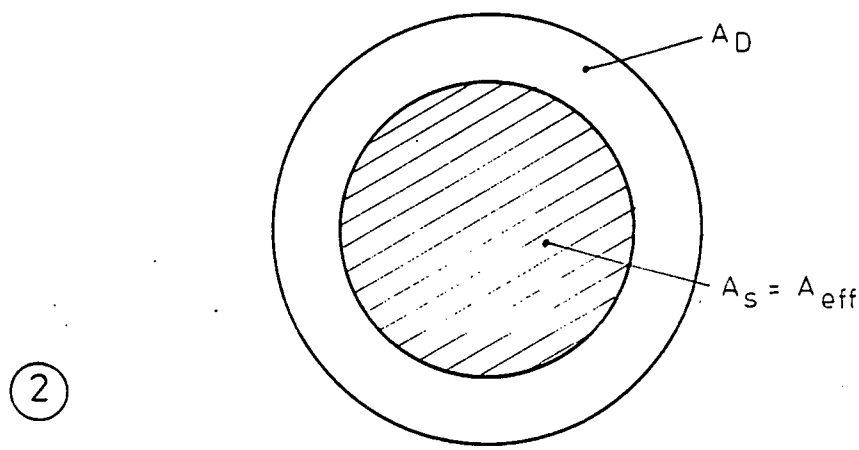

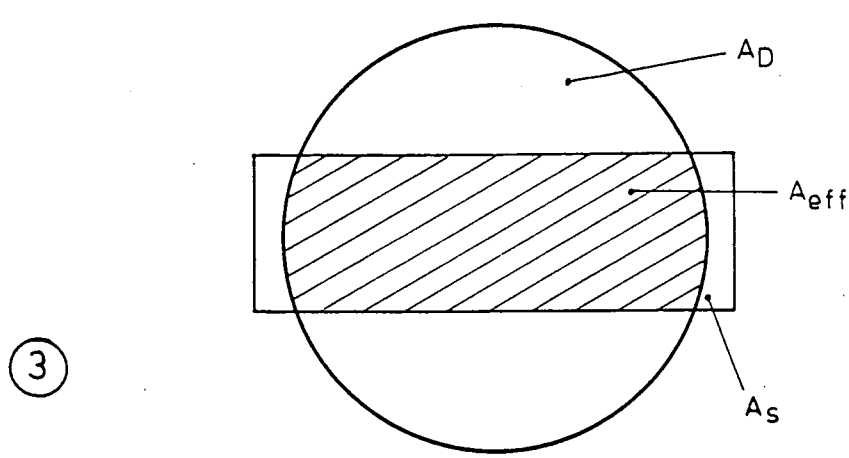

Figure 2.3: Effective areas (shaded in the figures).

The corresponding solid angle at A_{eff} is called Ω_{eff}. In the first case, the power measured is $P = B\,\Omega_d\,A_d$. In the second case, radiation is detected within a part of Ω_d. Now the power is most accurately expressed by $P = B\,\Omega_s\,A_d$. The third case is only applicable if the radiating object is imaged (sharply) on the detector. Then the effective cross section of Ω_d and Ω_s can be calculated. However this case is not likely to happen frequently and hence will not be discussed. The value of the product of area and solid angle in the above formula's for P is not fully correct. The exact value of $\Omega_{eff}\cdot A_d$ has to be calculated from:

$$\Omega_{eff}\cdot A_d = \iint_{A_d A_s} \frac{d\bar{A}_d(\bar{p})\;\bar{r}(\bar{p},\bar{q})\;d\bar{A}_s(\bar{q})\;\bar{r}(\bar{p},\bar{q})}{|r(\bar{p},\bar{q})|^4} \qquad (2.11)$$

(see figure 2.4), where $d\bar{A}_d$ is an infinitesimal area on the detector with coordinate $\bar{p}$ and $d\bar{A}_s$ is an infinitesimal area on the radiating surface with coordinate $\bar{q}$,

$$\bar{r}(\bar{p},\bar{q}) = \bar{p} - \bar{q} \qquad (2.12)$$

In practice we will use for the solid angle:

$$\Omega = \frac{A}{r^2} \qquad (2.13)$$

where $r^2 = |\bar{r}(\bar{p},\bar{q})|^2$ A_d, A_s,

and A is the radiating area, if the dimensions of the detector and object surfaces, with areas A_d and A_s respectively, are small compared to r.

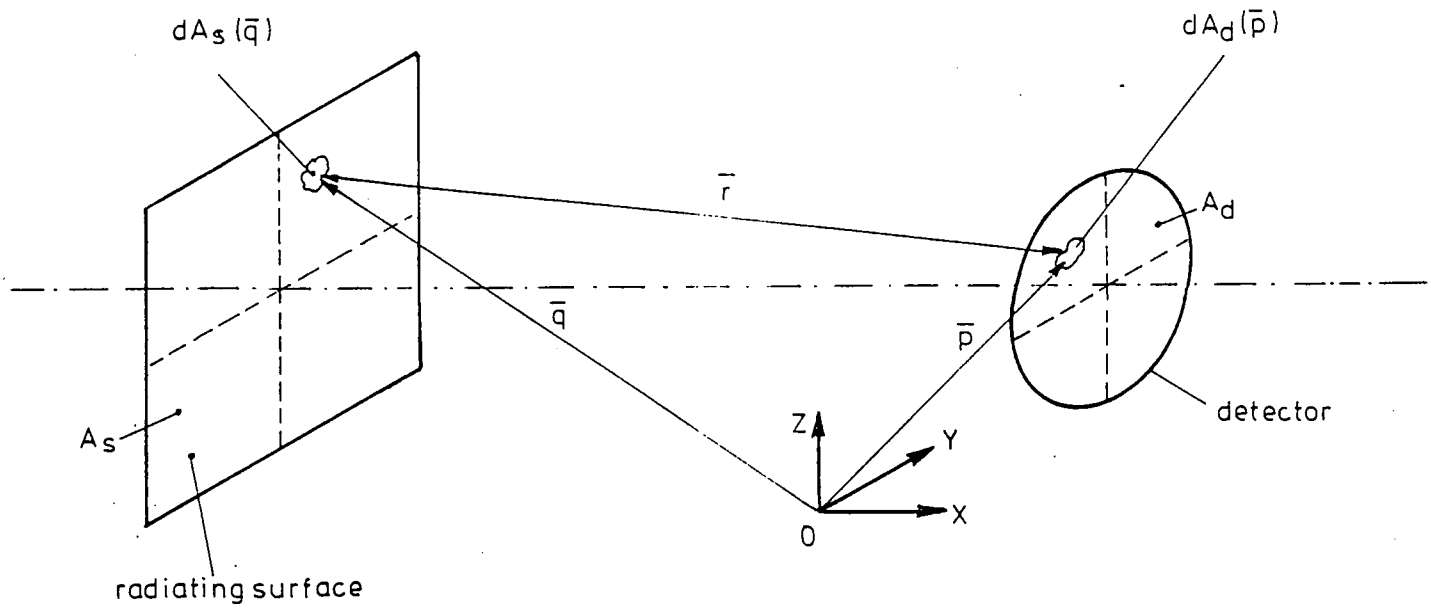

Figure 2.4: Surfaces and coordinates for the calculation of $\Omega_{eff} \cdot A_d$ (see par. 2.2).

2.3. The spectral transmission of plexiglas

A radiant beam incident on a specific medium is reflected at, absorbed in and transmitted through that medium. The ratio of the reflected to the incident spectral power is called reflectivity ρ_λ, the ratio of absorbed to incident spectral power is called absorptivity α_λ, and the ratio of transmitted to incident spectral power is called transmittivity τ_λ.
The reflectivity ρ_λ, at normal incidence at one intersection between the specific medium and the surrounding medium, is described by the Fresnel formula:

$$\rho_\lambda = \left(\frac{n_1 - n_2}{n_1 + n_2}\right)^2 \tag{2.14}$$

where n_1 and n_2 are the refractive indices for both media.
It appears from Fresnels theory, as expressed in (2.14), that the reflection only depends on n_1 and n_2 but not on the order the two media are traversed. As a result follows:

$$\tau_{\lambda r} = 1 - \rho_\lambda \tag{2.15}$$

where $\tau_{\lambda r}$ is the transmittivity at one intersection between the specific medium and the surrounding medium.
Spectral transmittivity $\tau_{\lambda b}$ in the bulk of the medium can be calculated from the following relation:

$$\tau_{\lambda b} = e^{-k_\lambda s} \tag{2.16}$$

where k_λ is the spectral absorption per unit of length and s is the pathlength.
The spectral transmission of a radiant beam incident on a medium is explained with help of figure 2.5 where a piece of the specific medium with thickness s is shown. The incident spectral power is $I_{\lambda,o}$.
At the intersection from the surrounding medium to the specific medium $I_{\lambda_1 r}$ is reflected and $I_{\lambda_1} = \tau_{\lambda r} I_{\lambda_o} = (1 - \rho_\lambda) I_{\lambda_o}$ is left. In the bulk of the medium (spectral) radiative power is absorbed. At the second intersection the spectral power is $I'_{\lambda_2} = I_{\lambda_o} (1 - \rho_\lambda) e^{-k_\lambda s}$.
At the transition from the specific medium to the surrounding meadium $I_{\lambda_2 r}$ is reflected and the spectral power $I_{\lambda_2} = I_{\lambda_o} (1 - \rho_\lambda)^2 e^{-k_\lambda s}$ is leaving the medium.

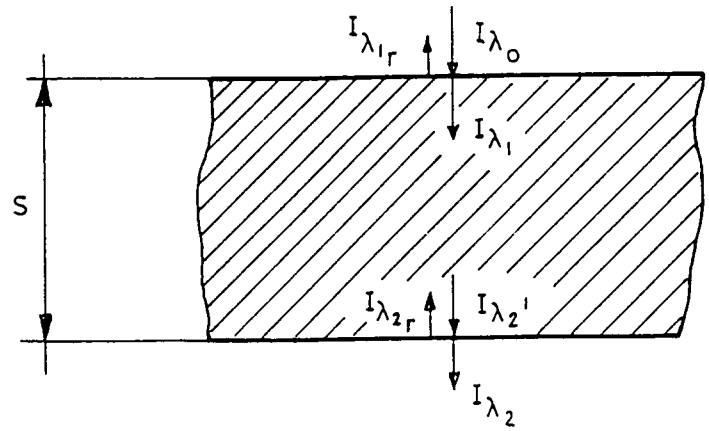

Figure 2.5: Decrease of spectral power of a radiant beam traversing a medium.

Hence the spectral power of a beam that has traversed a medium with thickness s becomes:

$$I_\lambda(s) = I_{\lambda_o}(1 - \rho_\lambda)^2 e^{-k_\lambda s} = I_{\lambda_o} \tau_{\lambda_r}^2 \tau_{\lambda_b} = I_{\lambda_o} \tau_\lambda \qquad (2.17)$$

For plexiglas an index of refraction $n_p = 1.49$ is found (ref. 3), for air $n_a = 1$. Hence from (2.14) follows $\rho_\lambda = 0{,}039$ or $\tau_{\lambda_r} = 0.961$ and from (2.17) $I_\lambda(s) = 0.924\ I_{\lambda_o} e^{-k_\lambda s}$ The spectral absorption per unit of length k_λ can and will be determined by measurement.
Of course k_λ and τ_λ vary with the wavelength λ, so a 'mean' value defined by the detector between 450 and 950 nm of these quantities will be found.

2.4. Solid fuel combustion chamber

The spectral radiation intensity distribution of gases is not equal to that of a blackbody of the same temperate. The intensity may look like figure 2.6.

The detector output is proportional to the spectral area between λ_1 and λ_2. It is obvious that this spectral area is smaller in the spectrum of the gas than in the spectrum of a blackbody with the same temperature. The detector will be calibrated on a tungsten-filament lamp with known ε_λ: 0,4 - 0,5. Since the emission factor of the flame in the SFCC is much lower ($\varepsilon = 10^{-2} - 10^{-4}$), the latter low value for ε has to be taken into account.

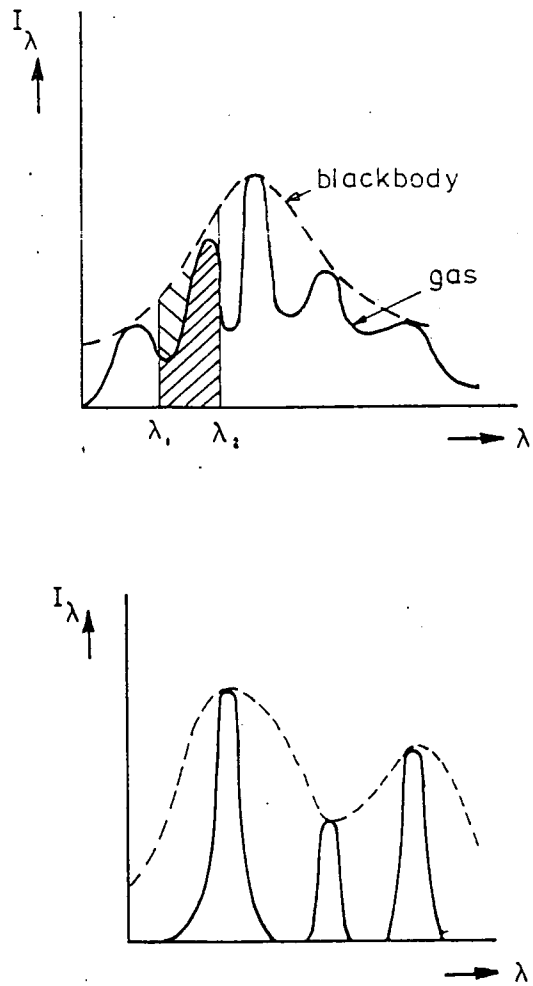

Figure 2.6: Possible spectral intensity distribution of the detected radiation.

As the radiation has to traverse the plexiglas wall of the cylinder also decrease of radiation through the wall, described by (2.17) must be taken into account.

3. THE DETECTOR

3.1. Geometry of the detector

In the previous paragraphs the detector is only treated as a certain area A_d, that can detect radiation within a certain solid angle Ω_d in a certain wavelength range.
In the following, the detector as it will be called, comprises a fotocamera, provided with a light sensitive diode (instead of a film) in the focal plane of the objective.
Instead of A_d, now A_ℓ, the lens area is relevant, together with the solid angle of acceptance Ω_d (see figures 3.1a and b), defined by the area of the diode and the focal length of the objective.

3.2. Equipment and experimental set up

The output current of the diode is proportional to the irradiated power, and is in the order of microamps per microwatts of irradiation. The spectral response reaches from 450 nm to 950 nm, and is almost flat.
The detector is mounted at the backside of the camera, in the focal plane of the objective. The output current is led to the amplifier. The amplified signal is measured with a voltmeter, see appendix A.
The effective diaphragm opening of the camera lens can be adjusted at several positions. The diaphragm number, indicated on the camera, should be equal to the focal length divided by the diaphragm opening. The exact diaphragm opening will be determined later. Change in diaphragm only causes a change in the amount of light, irradiating the detector.
When measurements are being carried out the shutter of the camera is continuously open. This makes measurement of changes in radiation feasible, as will occur at the SFCC. The whole set up is shown in figure 3.2.
More specific information about the equipment used is given in appendix A.

3.3. Sensitivity and saturation of the detector

Testing the equipment, it appeared that background radiation could be kept small; circa 2 mV output while the resolution of the voltmeter was 1 mV. The sensitivity of the diode, amplifier, voltmeter system was limited by the resolution of the voltmeter. The maximum output of the amplifier is 13.40 mV, hence the detector, combined with this amplifier can be saturated.

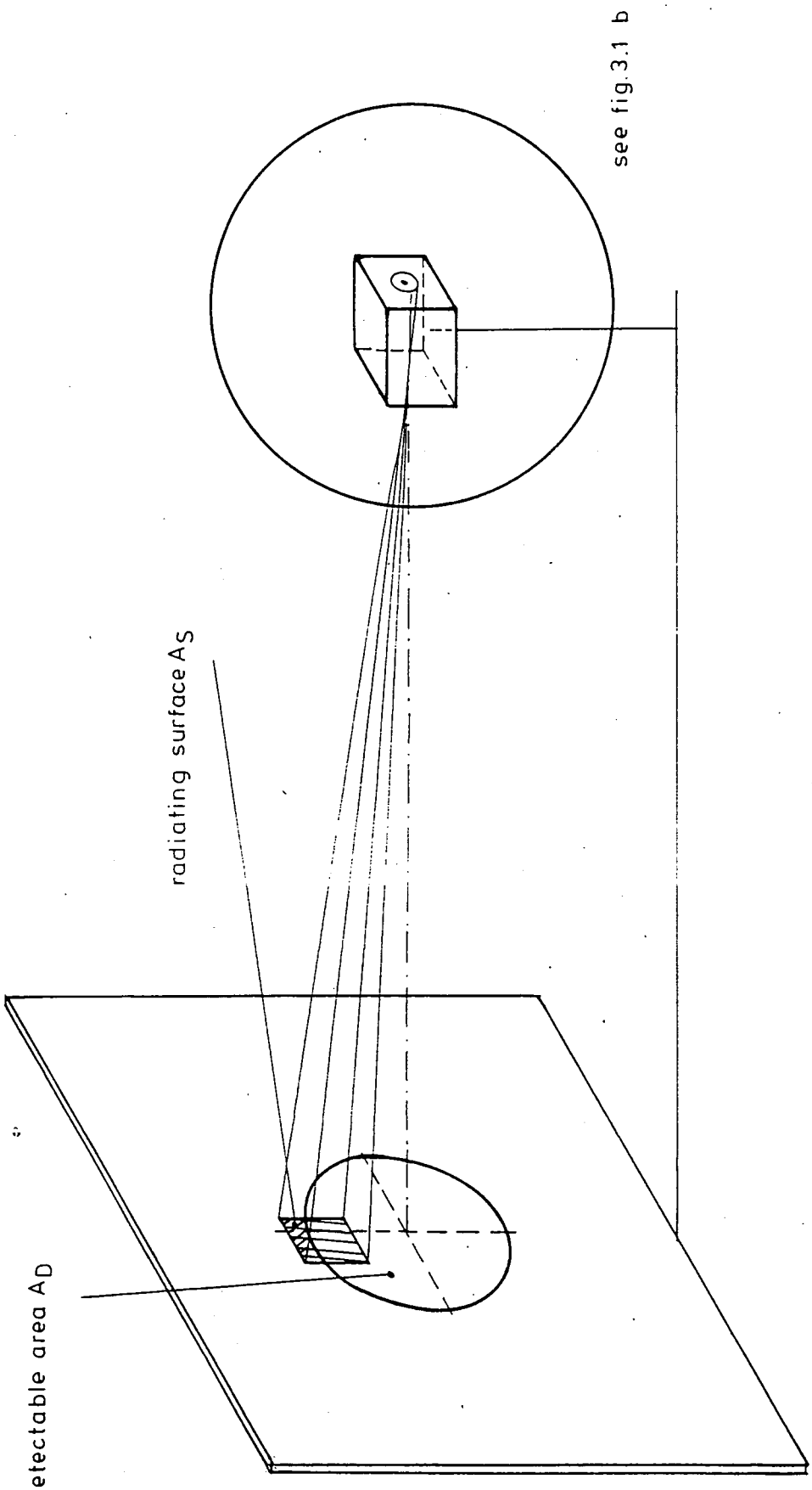

Figure 3.1a: Detection geometrics.

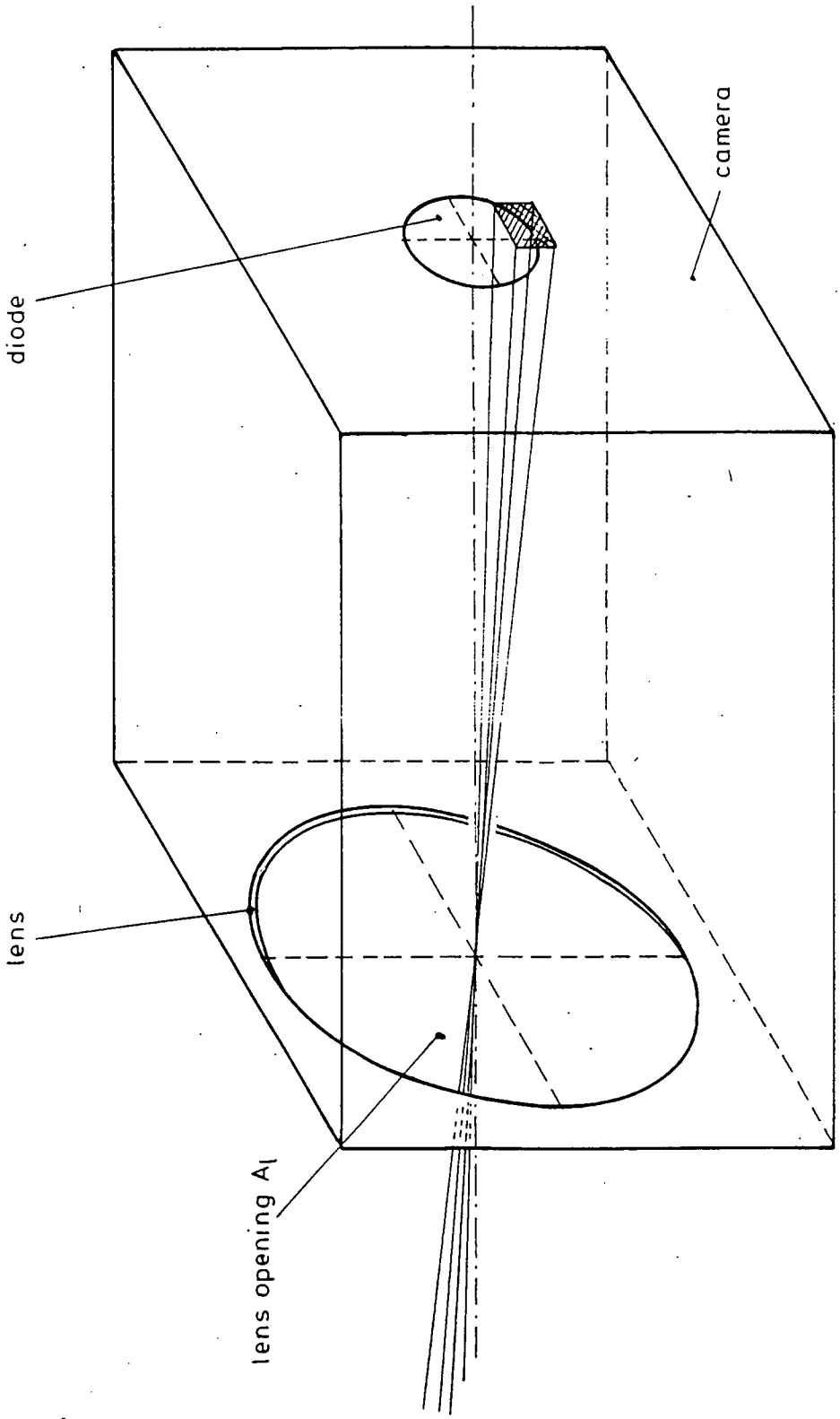

Figure 3.1b: Detection geometrics.

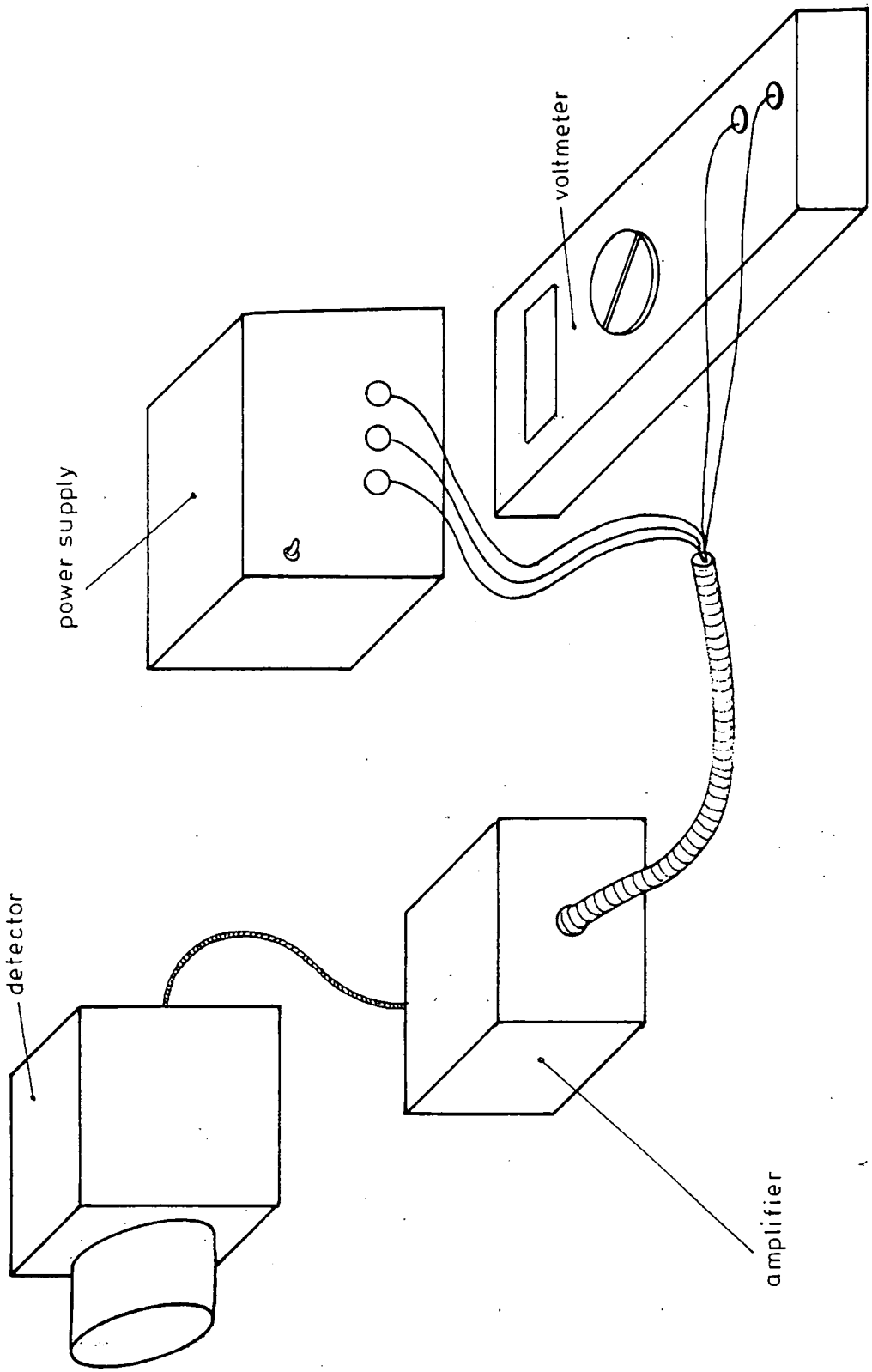

Figure 3.2: Set up for radiation measurement.

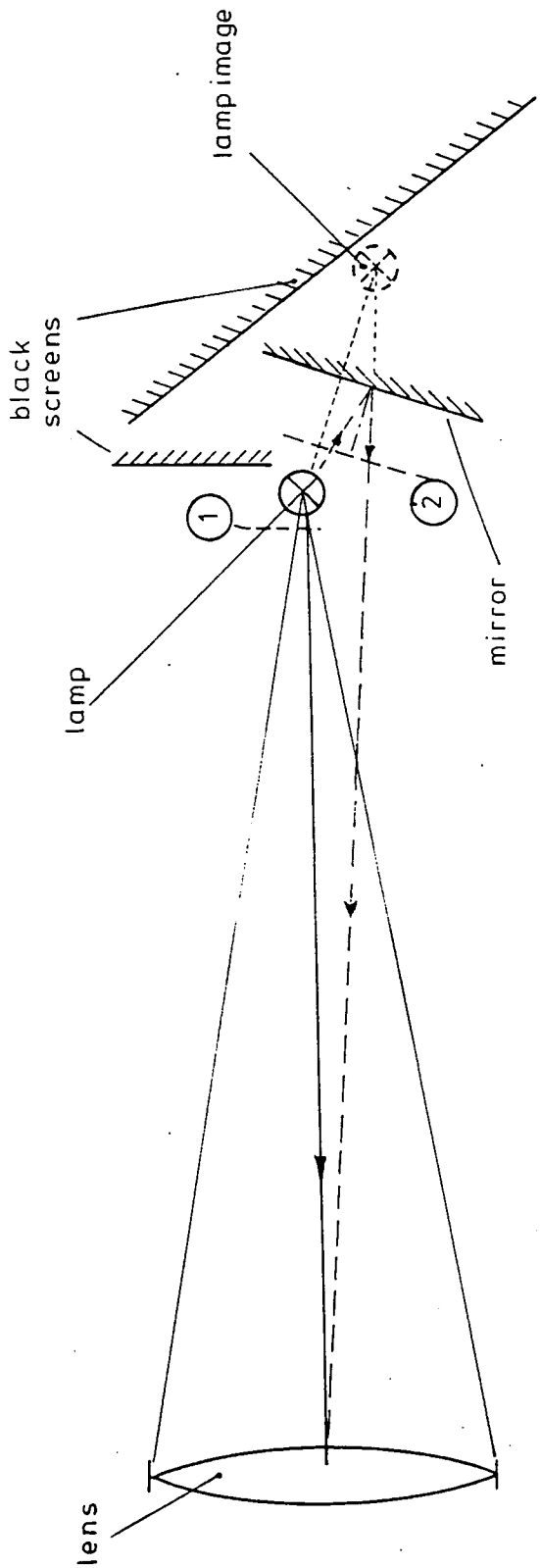

Figure 3.3: Saturation measurement.
Screen 1 screens off lamp radiation only.
Screen 2 screens off the radiation of the lamp image only.

To determine at what output voltage saturation pratically begins, a set up as drawn in figure 3.3 was built.
The detector was put in front of a lamp. A mirror was placed near the lamp so that also rays coming from the lamp were reflected via this mirror to the detector. Several black shields were placed to avoid undesired reflections being detected. The lamp was connected to a stabilised power supply of which the electric current and hence the lamp intensity could be varied.
The camera was adjusted so that the image of the lamp and the reflection on the diode were fairly sharp. It was made sure that both lamp and mirror were within the detectable area. The diaphragm number chosen was 5.6. The procedure to find the amount of saturation was the following:

1. Measurement of the amplifier output U_1 when only the light of the lamp was detected (and the light from the mirror was completely screened off).
2. Measurement of the output U_2 when only the contribution via the mirror was detected.
3. Measurement of the output U_3 when both lamp and reflection of the mirror irradiated the detector.
4. Measurement of the output U_4 when only the background contribution was detected by covering both lamp and mirror.

Covering the lamp or the mirror had to be done very carefully in order to avoid undesired reflections and not to obstruct rays to be measured.
The detector is (partly) saturated when:

$$U_1 + U_2 - 2U_4 > U_3 - U_4 \tag{3.1}$$

where U is the output voltage.
The amount of saturation can be found with:

$$\Delta U = U_1 + U_2 - U_3 - U_4 \tag{3.2}$$

if saturation at output voltage U_1 as well at U_2 is negligible. ΔU is the amount of saturation of the detector. By varying the electric current through the lamp, the amount of saturation is determined as a function of the indicated output voltage U, see figure 3.4.

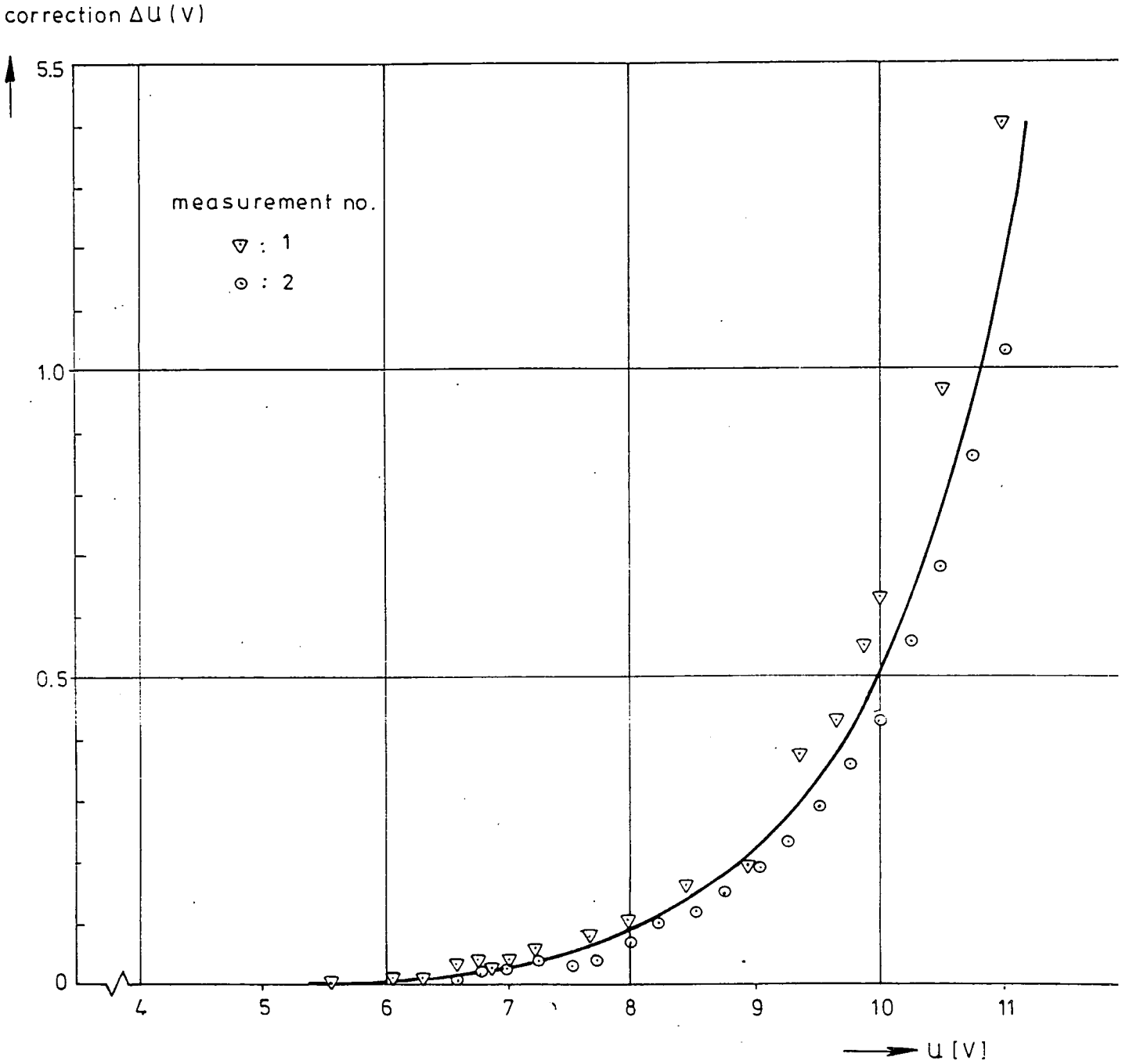

Figure 3.4: Saturation ΔU as a function of the indicated output voltage U. The correct output (proportional to the irradiated power) is U + ΔU.

The voltage U_{TRUE} corresponding to the amount of light power irradiating the detector is:

$$U_{TRUE} = U + \Delta U \tag{3.3}$$

Regarding the saturation curve and considering unavoidable errors, calculated in advance, it is sensible not to exceed an indicated output voltage of 7 V, where saturation is increased to one percent of the output signal.

3.4. Determination of the maximum area of the lens opening

As already stated the amount of light power irradiating the diode is proportional to the area of the effective lens opening. However this area is not known exactly. The effective diameter of the lens with diaphragm number 2.8 will be measured directly, because the shape of the diaphragm then is circular and has the smallest relative error in area.
For measuring the exact diameter of the effective lens opening at number 2.8 a HeNe laser was used, with its beam parallel to the optical camera axis. The camera was put on a table of which the height could be adjusted precisely (see fig. 3.5).
First via a lens the laserbeam was focused on the lamels of the diaphragm. Next, after moving the camera vertically, both camera locations where the focused laserbeam just struck the diaphragm were measured with a calliper.

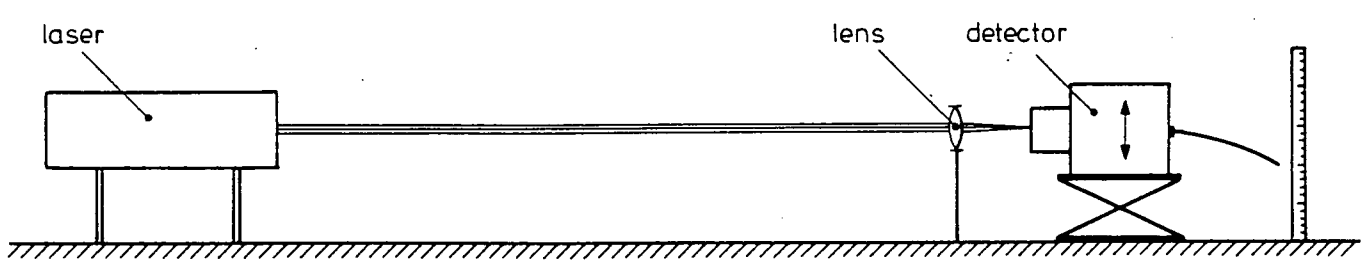

Figure 3.5: Set up for the determination of the diaphragm opening.

In order to check if the lens was centered well on the optical axis, the camera was moved and rotated slightly. If all the reflections were on one straight vertical line, the laserbeam was in the vertical plane through the optical axis

of the objective.
The diaphragm edge was assumed to be a perfect circle. Since the beam traversed the centre of the objective, the effective diameter was equal to the distance between the camera locations where the focused laserbeam just struck the diaphragm.
A series of measurements was carried out, each after readjustment, at diaphragm number 2.8, to derive the adjustment error.
For the effective diameter of the lens opening and adjustment error was found:

$$d_l = 27.8 \text{ mm} \pm 0.4 \text{ mm},$$

and hence for the area of the lensopening A_l:

$$A_l = 607 \text{ mm}^2 \pm 15 \text{ mm}^2.$$

3.5. Diaphragm adjustment

For each of the higher diaphragm numbers the mean area of the lens opening and the standard deviation in one adjustment will be determined now. All values will be determined with respect to the value at diaphragm number 2.8, of which the area of the opening is known already.
The experimental set up is simple: the detector measures the radiation of a lamp fed by a stabilised power supply, and the output signal is measured with a voltmeter.
Care has been taken that the detector did not get saturated (see par. 3.3) and background radiation was eliminated.
Since the lamp was focused on the diode each point of the lamp corresponded to a point of the image on the diode. Now, when only the diaphragm is changed, the change in output signal is proportional to the change in lens opening area, since the distance from lens to lamp is much larger than the radius of the effective lens opening.

Three series of measurements were carried out, each series for a different current through the lamp. From the results the detector was found to be linear within the limits of accuracy.
For each diaphragm number the mean output voltage of the detection system and its standard deviation were determined. These mean output voltages were divided by the mean output voltage values at diaphragm number 2.8 and also the standard

deviations of these ratio's were determined for the three series of measurements. The results are presented in table 3.1, where the area of each lens opening and its error is given for the different diaphragm numbers. It can be concluded that it is preferable to use large openings.

Δ	$A/A_{2.8}$	A [mm^2]	σ/A	σ [mm^2]
2.8	1	607.0	2.5%	15.3
3.4	0.710	431.0	3.4%	14.7
4	0.513	311.4	3.8%	11.8
4.8	0.363	220.3	4.4%	9.7
5.6	0.256	155.4	5.0%	7.8
6.7	0.180	109.3	5.1%	5.6
8	0.129	78.3	5.3%	4.1
9.5	0.091	55.2	6.0%	3.3
11	0.064	38.8	6.8%	2.6
13.5	0.045	27.3	7.2%	2.0
16	0.032	19.4	6.8%	1.3
19	0.023	14.0	5.1%	0.7
22	0.017	10.3	6.4%	0.7

Table 3.1: Lens openings for different diaphragm numbers.

3.6. Determination of focus, focal distance and principal plane

When the camera is used, it is necessary to know the focal distance and the locations of the focal planes, and of the principal plane of the object space. This principal plane is the reference plane for measuring the distance between the object and the camera lens. The distance between a principal plane and a focal plane, both belonging to the same space, is the focal distance f.
The focal plane at the diode was located 3 mm behind the camera reference plane to which the diode holder was attached. For the determination of the focal distance f the following set up was built, figure 3.6.

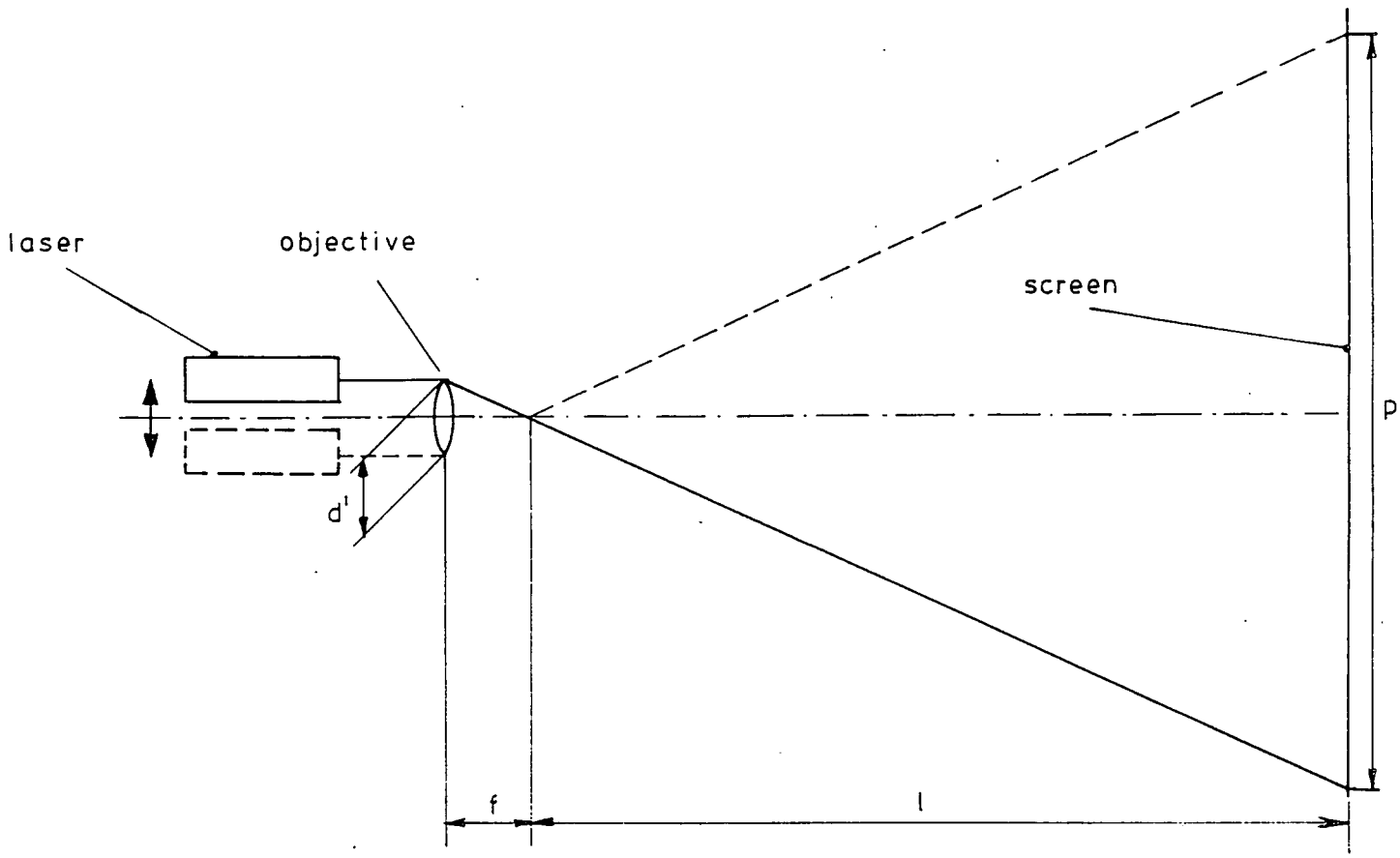

Figure 3.6: Geometrics for the determiation of the focal distance of the objective.

The camera was mounted with its optical axis parallel to a laserbeam. This laserbeam was translated in a horizontal plane through the optical axis of the camera over distance d'. The spot of the laserbeam, formed by the camera objective on a screen at known distance l behind the focal plane of the camera lens, consequently moved along distance p.
The focal distance f follows from:

$$f = \frac{d' . l}{p} \qquad (3.4)$$

In this set up l = 2096 mm ± 1 mm.
The accuracy of the determination of f was limited by the relative error in the measurement of d' (ca 0.2% for one measurement).
The following result from successive measurements of d' and p could be obtained:

$$f = 80.2 \pm 0.4 \text{ mm}$$

on the optical axis and for a lens region at 13 mm from this axis. Optical errors were ignored here, regarding the high quality of the objective.
From this result follows that the principal plane of the image space is located at 77 mm ± 0.5 mm in front of the camera reference plane.
The determination of the principal plane of the object space demands a different set up.
A mirror is mounted at the image side of the objective, the exact location is not important. A light source and screen in the same plane perpendicular to the optical axis and in front of the objective, are adjusted along the optical axis in order to image the source on the screen, see figure 3.7.

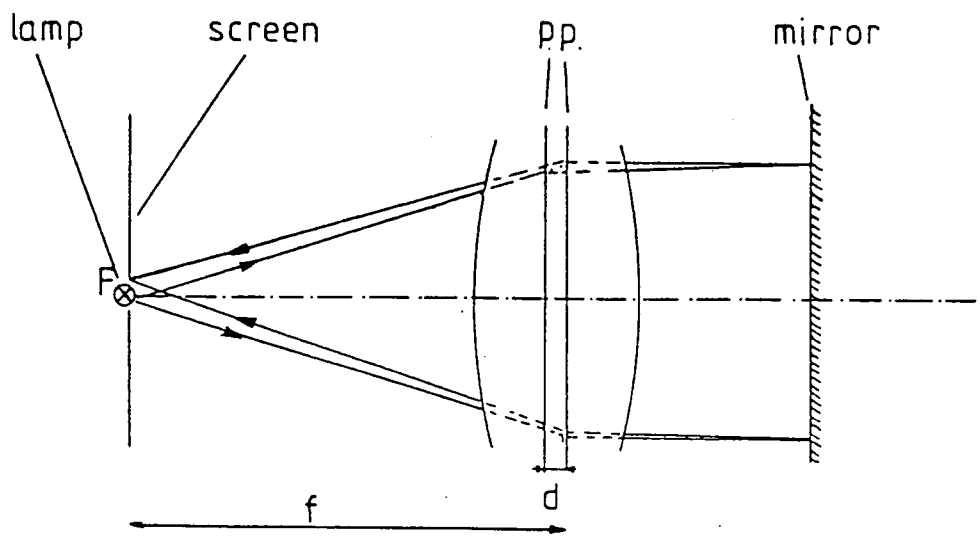

Figure 3.7: Geometrics for the determination of the principal plane of the object space.

With help of the above measured focal distance the principal plane of the object space is found to be (with sufficient precision) at 75 ± 0.5 mm in front of the camera reference plane. Effectively the lens must be regarded to be at this location when distances from objects to this lens are measured.
In figure 3.8 the two principal planes, the camera reference plane and the focal distance f are shown.

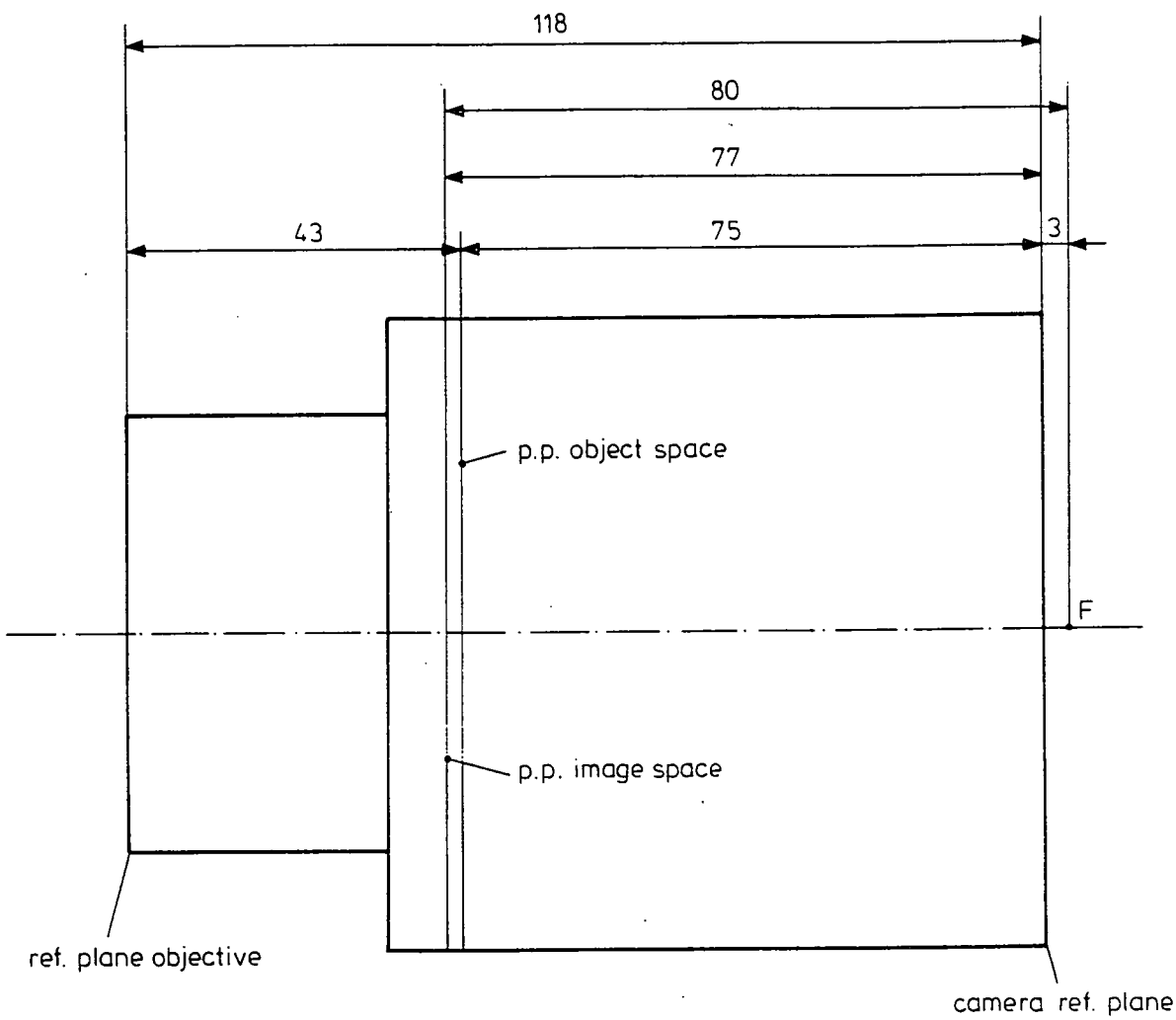

Figure 3.8: Locations of principal planes (p.p.), focal place through F and reference planes.

4. CALIBRATION OF THE DETECTOR

4.1. Calibration source

The calibration source is a calibrated tungsten ribbon lamp, for calibration data see table 4.1.

i [A]	T_{TRUE} [K]	B_{λ_1,λ_2} [$Wm^{-2}\ sr^{-1}$]	$B_{\lambda_1,\lambda_2,m} = 0.92\ B_{\lambda_1,\lambda_2}$ [$Wm^{-2}\ sr^{-1}$]
5.31	1400	$1.55 \cdot 10^2$	$1.43 \cdot 10^2$
5.51	1450	$2.35 \cdot 10^2$	$2.16 \cdot 10^2$
5.73	1500	$3.46 \cdot 10^2$	$3.18 \cdot 10^2$
5.96	1550	$5.00 \cdot 10^2$	$4.60 \cdot 10^2$
6.21	1600	$7.06 \cdot 10^2$	$6.50 \cdot 10^2$
6.74	1700	$1.33 \cdot 10^3$	$1.22 \cdot 10^3$
7.32	1800	$2.36 \cdot 10^3$	$2.17 \cdot 10^3$
7.94	1900	$3.93 \cdot 10^3$	$3.62 \cdot 10^3$
8.58	2000	$6.27 \cdot 10^3$	$5.77 \cdot 10^3$
9.23	2100	$9.62 \cdot 10^3$	$8.85 \cdot 10^3$
9.90	2200	$1.42 \cdot 10^4$	$1.31 \cdot 10^4$
10.60	2300	$2.04 \cdot 10^4$	$1.88 \cdot 10^4$
11.33	2400	$2.84 \cdot 10^4$	$2.61 \cdot 10^4$
12.08*	2500	$3.88 \cdot 10^4$	$3.57 \cdot 10^4$
12.85**	2600	$5.18 \cdot 10^4$	$4.77 \cdot 10^4$

Table 4.1: Radiance between λ_1 = 450 nm and λ_2 = 950 nm of a tungsten ribbon lamp as a function of the true temperature T_r and current i.

Lamptype W2KGV22i nr. 1920
Calibration : May 1964
Recalibration: February 1969
Window transmission: 0.92

* February 1969 12.12 A
** February 1969 12.89 A

From the temperature, the spectral intensity per unit of area is calculated with Planck's formula (2.1) and with the emissivity ε (literature).
To integrate the spectral intensity over the wavelength range from 450 to 950 nm, this interval is divided in 10 intervals and a Simpson's approximation has been carried out.
The relative accuracy of this approximation is far better than the relative accuracy of the final calibration will be (3%).
For each temperature the radiance of the filament between λ_1 = 450 nm and λ_2 = 950 nm is found from (see par. 2.2):

$$B_{\lambda_1,\lambda_2} = \int_{\lambda_1}^{\lambda_2} B_\lambda \, d\lambda = \int_{\lambda_1}^{\lambda_2} B_{b,\lambda} \, \varepsilon_\lambda \, d\lambda = \frac{1}{\pi} \int_{\lambda_1}^{\lambda_2} I_{b,\lambda} \, \varepsilon_\lambda \, d\lambda \qquad (4.1)$$

As the light has to traverse the lamp window, the radiance to be measured outside the lamp, indicated with an index m, is 92% of the calculated radiance inside the lamp, according to the specifications.
In table 4.1 both the calculated radiance, B_{λ_1,λ_2}, and the radiance to be measured outside the lamp, $B_{m,\lambda_1,\lambda_2}$, are given as a function of the electric current I and of the real temperature T.

4.2. Calibration set up

The whole set up is built on a large stone table, see figure 4.1.
The lamp is connected to a stabilised power supply of which the current can be varied precisely. The current is measured by measuring the voltage, amplified 202.0 ± 0.1 times, over a precision resistor of $10^{-3} \pm 10^{-6}$ Ω.
The radiating part of the lamp, the filament, is a small tungsten ribbon, about 2 mm in width. A pointer indicates the location of calibration on the filament. Only this part of the filament was used for the detector calibration, by applying an adjusted horizontal slit in front of the lamp. This slit also screened off any other disturbing reflections from the lamp.
To prevent detection of stray light from the lamp environment a black hardpaper box with a hole was put around the lamp. Care has been taken that the air in the box did not get heated. Between the detector and the lamp two extra black screens with holes were placed, to reduce residual background radiation.

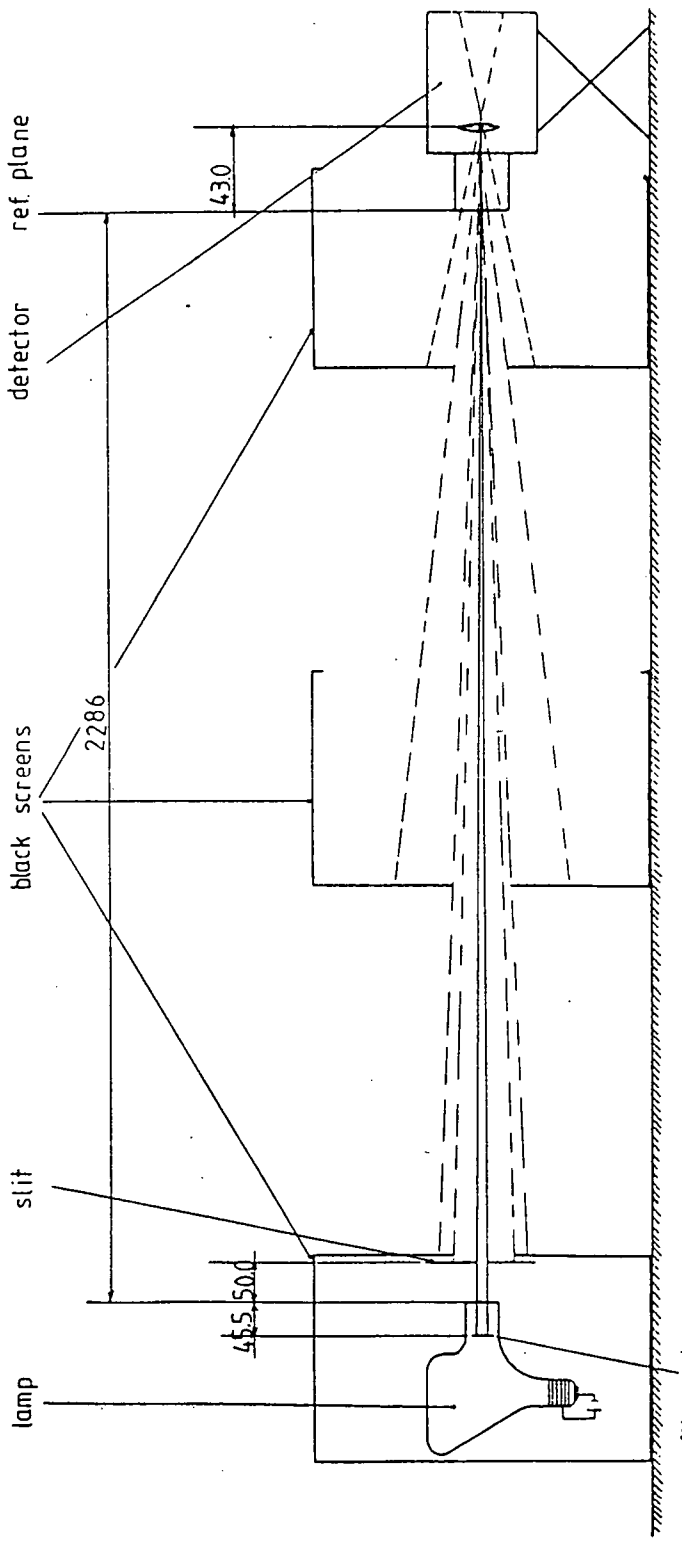

Figure 4.1: Calibration set up. Figures for the distances apply to measurement series no. 1.

4.3. Calibration geometrics

The calibration constant C follows from equations (2.6), (2.8), (2.9) and (2.10):

$$C = \frac{E_{c,\lambda_1,\lambda_2} \cdot r_c^2}{B_{c,\lambda_1,\lambda_2,m} \cdot A_1 A_s} = \frac{E_{c,\lambda_1,\lambda_2}}{P_{c,\lambda_1,\lambda_2}} \qquad (4.2)$$

From this equation follow the quantities to be measured for a proper calibration (see fig. 4.1):

- r_c, the distance between filament and principal plane of the objective,
- A_s, the radiating area, as projected on the filament, which will be found from:
  - the height of the slit
  - the width of the filament
  - the distance between slit and filament
  - r_c
- A_1, the lensopening area, see table 3.1.

The width of the filament was determined with help of a laser. The laserbeam was sharply focused on the filament with a lens.
The lamp could be moved perpendicular to the laserbeam. The distance between the two lamp positions where the focused laserbeam just hit the filament, was found to be 2.13 ± 0.02 mm.
No expansion of the filament was detected after the lamp was switched on.
With the same method the distance along the optical axis between filament and slit was found to be 95.5 ± 0.3 mm.
The distance lamp window-reference plane of objective was 2286 ± 1 mm, see fig. 4.1.
This made the distance r_c, between the filament and the principal plane to be 2374.5 mm.
The height of the slit was measured with a calliper. A height of 2.08 ± 0.01 mm was found from a series of measurements.
The projected height of the radiating area on the filament then was:

$$(2.08 \pm 0.01) \cdot \frac{2374.5}{2279} = 2.17 \pm 0.01 \text{ mm.}$$

Hence the radiating area A_s was 2.17 x 2.13 = 4.62 ± 0.05 mm^2.

4.4. Calibration procedure and results

Calibration measurements were carried out for two lens openings and for two distances r_c.
The lamp was adjusted to a specific temperature by feeding the lamp with the proper current (see par. 4.2).
For each temperature the detector output voltage E_{λ_1,λ_2} was measured. From each series background radiation was subtracted.
The results of these measurements can be found in appendix B.
With help of a linear regression method the best fitting line through the origin is found. The slope of this line is the constant C (see fig. 4.2).
According to equation 4.2:

$$C = \frac{E_{\lambda_1,\lambda_2} \cdot r_c^2}{B_{\lambda_1,\lambda_2} \cdot A_s \cdot A_1} \qquad (4.2)$$

errors in the measurement of E_{λ_1,λ_2}, B_{λ_1,λ_2}, r_c, A_1 and A_s will reduce the accuracy of the determination of C.
The deviation of the $E_{\lambda_1,\lambda_2} - P_{\lambda_1,\lambda_2}$ graph from a straight line for small values of P_{λ_1,λ_2} (see fig. 4.2) may be caused by:

1. The inhomogeneous spectral response of the diode, in the wavelength range of 450 to 950 nm. As for increasing temperature the lamp spectrum changes, the power response of the detector $\frac{\Delta P_{\lambda_1,\lambda_2}}{\Delta E_{\lambda_1,\lambda_2}}$, changes.
2. The calibration of the lamp can systematically be incorrect for low temperatures. An error of 5 K in temperature causes an error of 2 to 3 percent in radiance.
3. The emissivity ε may systematically be incorrect, however measurements of ε claim an accuracy of 0.5% (literature).

Errors that influence the slope C of the line in figure 4.2 are:
1. The error in the area of the radiating surface, A_s, which is 1%.
2. The error in r_c^2, which is 0.2%.
3. The error in the area of the lensopening A_1, which is 2.5% at diaphragm number 2.8. See for errors of other diaphragms, table 3.1.
4. The error in the voltmeter which is 0.3%.

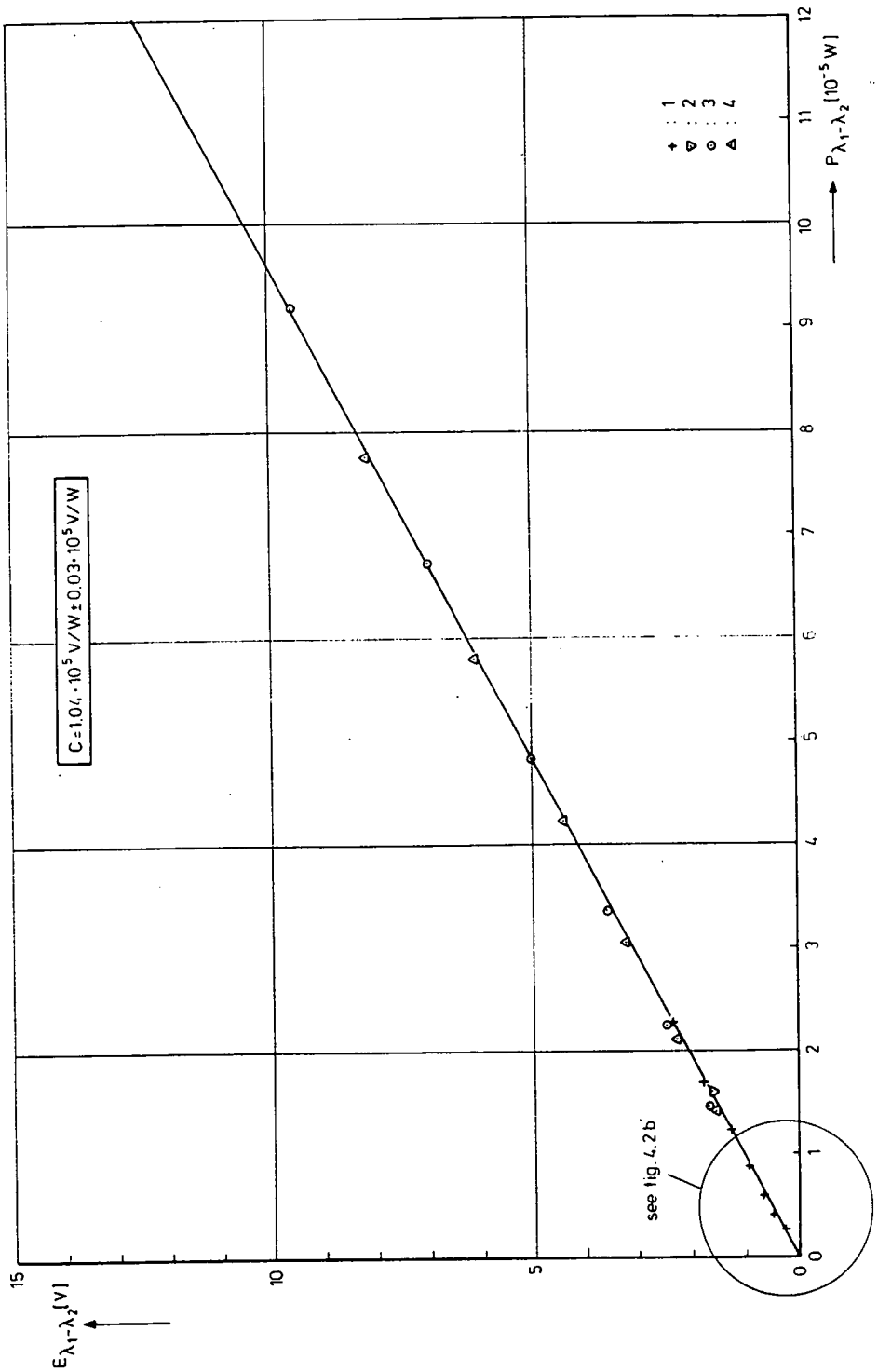

Fig. 4.2a: Calibration graph.

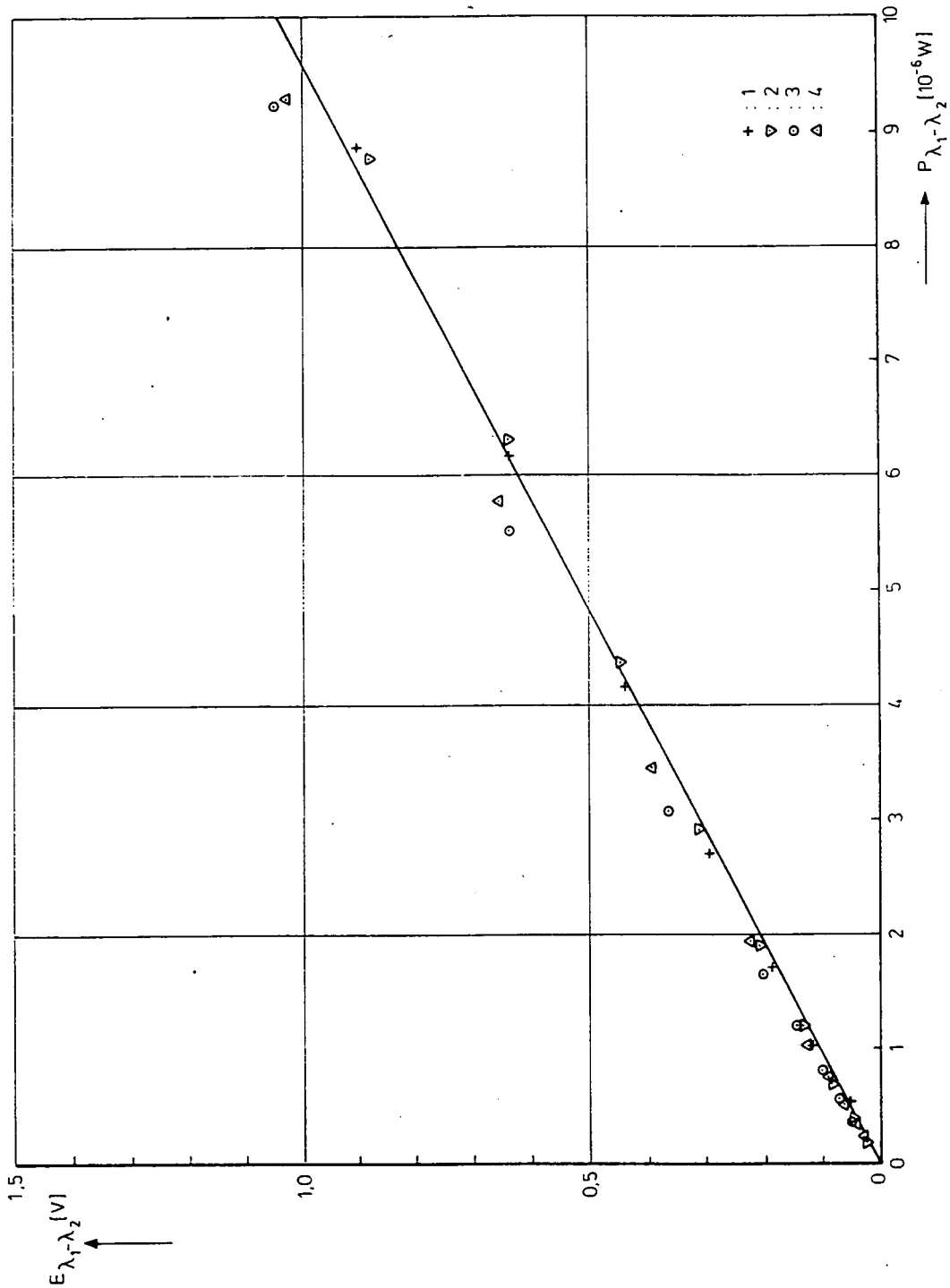

Fig. 4.2b: Calibration graph.

The error in the measurement of the lamp current is negligible.

The stochastical errors are:

1. The error in the output voltage E_{λ_1,λ_2} of 1 significant digit resulting in an error up to 0.3%.
2. The adjustment error of the lamp current, which is 0.005 A, causes a relative error up to 0.1% in temperature; hence up to 1% in radiance.

Gathering all systematical errors, the total systematical error in P_{λ_1,λ_2} becomes ($\Delta = 2.8$):

$$\sqrt{(1.0\%)^2 + (0.2\%)^2 + (2.5\%)^2 + (0.3\%)^2} = 3\%$$

In figure 4.2 only the stochastical errors are to be indicated in the calibration graph, but are very small.

The corresponding calibration constant C is:

$$C = 1.04 \cdot 10^5 \pm 0.03 \cdot 10^5 \text{ V/W}$$

5. MEASUREMENT ON A BUTANE FLAME

The applicability of the pyrometer method of temperature measurement was examined on a butane flame.

A piece of iron of 1 mm thickness was held in a butane flame. Care had been taken that the iron temperature was close to the flame temperature. The radiation of the metal is measured with the detector, while flame radiation is kept as low as possible.

The radiance B_{λ_1,λ_2} follows from equation 4.2:

$$B_{\lambda_1,\lambda_2} = \frac{E_{\lambda_1,\lambda_2}\, r^2}{C \cdot A_1 \cdot A_s} \qquad (5.1)$$

The experimental quantities were as follows:

$$E_{\lambda_1,\lambda_2} = 2.3 \text{ V} \pm 0.05 \text{ V},$$
$$r = 0.3575 \text{ m} \pm 0.0005 \text{ m},$$
$$A_1 = 607 \text{ mm}^2 \pm 15 \text{ mm}^2,$$
$$A_s = 9.6 \text{ mm}^2 \pm 0.1 \text{ mm}^2.$$

Hence $B_{\lambda_1,\lambda_2} = 4.85 \cdot 10^2 \text{ Wm}^{-2} \text{ sr}^{-1} \pm 0.18 \cdot 10^2 \text{ Wm}^{-2} \text{ sr}^{-1}$.

To find the temperature from the radiance in the wavelength range λ_1 = 450 nm and λ_2 = 950 nm, the assumption was made that the mean emissivity of iron in that region equalled that of tungsten at the same temperature, although it is presumably a little higher.

With help of table 4.1, a temperature of approximately 1550 K was found.

Measurement with a thermocouple showed a temperature of 1440 K.

Apart from the assumptions that are made, the difference in the two results might be caused by differences in radiative losses of iron and thermocouple.

6. CONCLUSIONS

In order to determine the temperature of flames, it is necessary to know, apart from directly measurable quantities, the emissivity ε in the detection wavelength range.

The detector calibration has been carried out with a precision of 3%, which is regarded to be sufficient in view of the poor knowledge of other emissivities. When the emissivity is not known at all, other methods like spectroscopic ones have to be used to determine the temperature. Spectroscopic measurements and measurements with the detector can be carried out simultaneously in order to find correlations between spectra, radiation intensity and the temperature determined.

Further study and experiments on this topic are required.

7. REFERENCES

1. P.A.O.G. Korting, H.F.R. Schöyer.
'Solid Fuel Combustion Chamber Research in the Netherlands'.
Report LR-444/PML 1984.C74, SFCC Publication no. 20, Delft University of Technology, Department of Aerospace Engineering/Prins Maurits Laboratory TNO, Delft/Rijswijk, September 1984.

2. E.R.G. Eckert, Robert M. Drake, jr.
'Analysis of Heat and Mass Transfer'.
McGraw-Hill Book Company, USA, 1972.

3. Robert C. Weast.
'Handbook of Chemistry and Physics'.
CRC Press Inc., Cleveland Ohio USA, April 1975.

4. R.S. Longhurst.
'Geometrical and Physical Optics', 3rd edition.
Longman, London, May 1972.

APPENDIX A

MEASURING EQUIPMENT

The measuring equipment consists of a PIN-diode mounted at the backside of a photocamera. The outputsignal of the diode is amplified by an amplifier and measured with a voltmeter, see figure 3.2.

The diode is an United Detector Technology Inc. PIN 10 DF diode, serial no. 51465. For further specifications see figure A1.

The camera is a Hasselblad 500 C, serial no. TU 75791. The lens is a Zeiss, 1:28, f = 80 mm. serial number 5658194.

The amplifier is feeded by a stabilised power supply. The scheme of the amplifier is shown in figure A2.

The resistor R_c of 825 kΩ is used to check or carry out the adjustment of the variable resistor R.

The amplification is adjusted (by resistor R) in such a way that a wide range of intensities to be expected could be measured at linear response.

Changes in amplification induce changes in the ratio of the voltage applied to resistor R_c and the output voltage and hence can be corrected easily when this ratio at proper amplification is known.

For calibration of the amplifier, a voltage of 3.000 V was applied to R_c resulting in an output voltage of 2.431 V.

This adjustment was used for all measurements described in this report. The voltmeter used was a Fluke 77 multimeter, serial number 3485233. Further specifications can be found in figure A3.

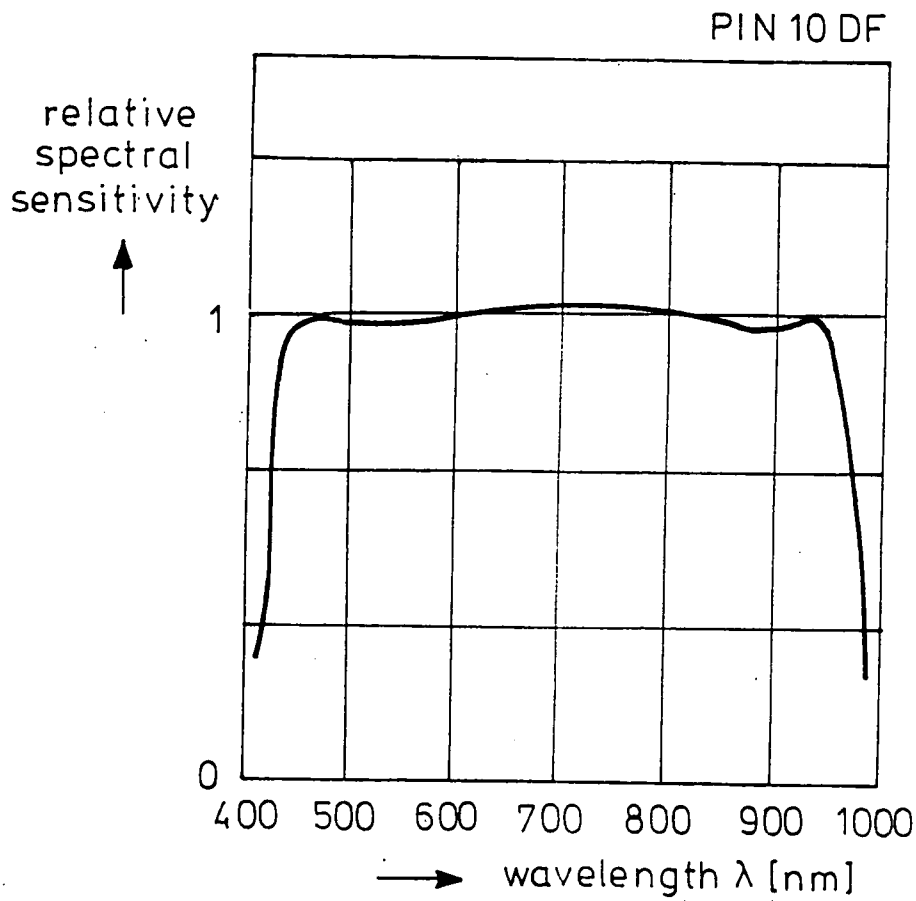

Figure A1: The spectral response of the PIN 10 DF.

The PIN 10 DF (DETECTOR/FILTER COMBINATION) produces a flat spectral response from 450 nm to 950 nm. This is the spectral response required for radiometric measurements, and is the response exhibited by thermopiles. The advantages of the PIN 10 DF are stability and sensitivity. The PIN 10 DF is a thousand times more sensitive than a thermopile, and ten times more stable than a thermopile. The PIN 10 DF can be calibrated in terms of microamps out per microwatts of light into the PIN 10 DF.

Characteristics: Linear Output : 10^{-11} W to 10^{-3} W
Frequency Response: DC to 15 MHz
Active Area : 1 cm^2

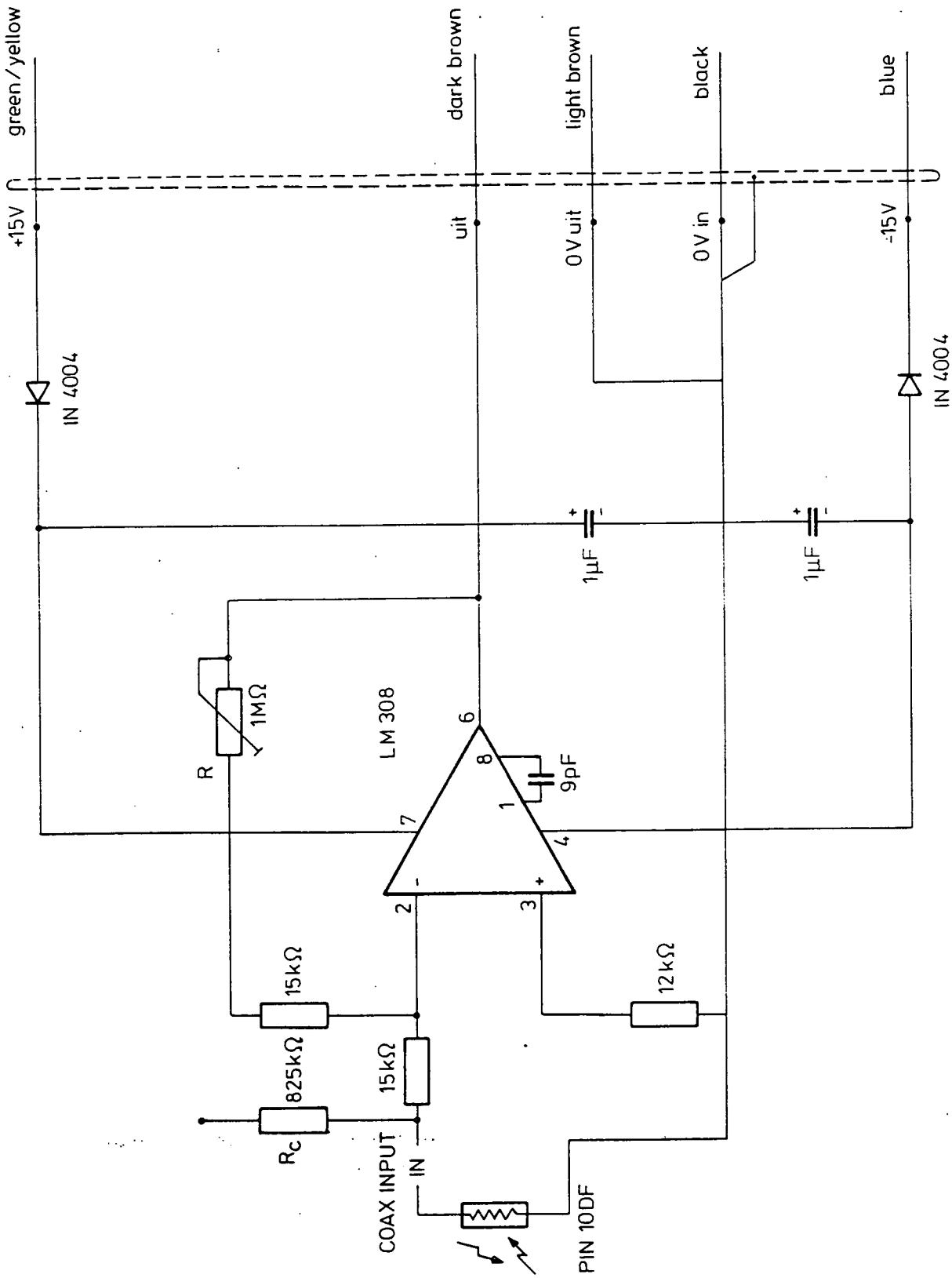

Figure A2: amplifier.

SPECIFICATIONS

Operating Temperature	0°C to 50°C
Storage Temperature	-40°C to +60°C
Relative Humidity	
All ranges except 32 MΩ	0% to 90% (0°C to 35°C) 0% to 70% (35°C to 50°C)
32 MΩ range only	0% to 80% (0°C to 35°C) 0% to 70% (35°C to 50°C)
Temperature Coefficient	0.1 x (specified accuracy)/°C (applies from 0°C to 18°C and from 28°C to 50°C)
Battery Type	NEDA 1604 9V or 6F 22 9V
Battery Life (typical)	1600 hrs Zn-C 2000+ hrs alkaline
Size (HxWxL)	2.84 cm x 7.49 cm x 16.64 cm (1.12 in x 2.95 in x 6.55 in)
Weight	0.34 kg (12 ounces)
Safety Rating	Protection Class II per IEC 348

FUNCTION	RANGE	RESOLUTION	ACCURACY (Fluke 75)	ACCURACY (Fluke 77)	FULL SCALE BURDEN VOLTAGE
V~ 45 Hz-1 kHz	3.2V	0.001V	±(2 + 2)*	±(2 + 2)*	
	32V	0.01V	±(2 + 2)	±(2 + 2)	
	320V	0.1V	±(2 + 2)	±(2 + 2)	
(*45-500Hz)	750V	1V	±(2 + 2)	±(2 + 2)	
V⎓	3.2V	0.001V	±(0.5 + 1)	±(0.3 + 1)	
	32V	0.01V	±(0.5 + 1)	±(0.3 + 1)	
	320V	0.1V	±(0.5 + 1)	±(0.3 + 1)	
	1000V	1V	±(0.8 + 1)	±(0.4 + 1)	
300mV⎓	320 mV	0.1 mV	±(0.5 + 1)	±(0.3 + 1)	
Ω	320Ω	0.1Ω	±(0.7 + 2)	±(0.5 + 2)	
	3200Ω	1.0Ω	±(0.7 + 1)	±(0.5 + 1)	
	32 kΩ	0.01 kΩ	±(0.7 + 1)	±(0.5 + 1)	
	320 kΩ	0.1 kΩ	±(0.7 + 1)	±(0.5 + 1)	
	3.2 MΩ	0.001 MΩ	±(0.7 + 1)	±(0.5 + 1)	
	32 MΩ	0.01 MΩ	±(2.5 + 1)	±(2.0 + 1)	
⊣◆))))]	2.0V	0.001V	±(1 + 1) typical		
A~ 45 Hz-1 kHz	32 mA	0.01 mA	±(3 + 2)	±(3 + 2)	0.16V
	320 mA	0.1 mA	±(3 + 2)	±(3 + 2)	2.0V
	10A	0.01A	±(3 + 2)	±(3 + 2)	0.5V
A⎓	32 mA	0.01 mA	±(1.5 + 2)	±(1.5 + 2)	0.16V
	320 mA	0.1 mA	±(2 + 2)	±(2 + 2)	2.0V
	10A	0.01A	±(1.5 + 2)	±(1.5 + 2)	0.5V

FUNCTION	MAXIMUM INPUT VOLTAGE (across input terminals)	RESPONSE TIME (of digital display to rated accuracy)	INPUT IMPEDANCE	COMMON MODE REJECTION RATIO (1 kΩ unbalance)	NORMAL MODE REJECTION RATIO (digital display only)
V~	1000V dc 750V ac rms (sine)	<2s	>10 MΩ in parallel with <50 pF (ac coupled)	>60 dB (dc to 60 Hz)	
V⎓	1000V dc 750V ac rms (sine)	<1s	>10 MΩ (input capacitance: <50 pF)	>120 dB (dc, 50 Hz, or 60 Hz)	>60 dB (50 or 60 Hz)
300mV⎓	500V dc 500V ac rms (sine)	<1s	10 MΩ (input capacitance: <50 pF)	>120 dB (dc, 50 Hz, or 60 Hz)	>60 dB (50 or 60 Hz)

MAXIMUM VOLTAGE BETWEEN ANY TERMINAL AND EARTH GROUND (all functions):
1000V dc 750V ac rms (sine)

FUSE PROTECTION (300 mA terminal only):
630 mA 250V FAST 3A 600V FAST

	MAXIMUM OVERLOAD (across input terminals)	RESPONSE TIME (of digital display to rated accuracy)	OPEN CIRCUIT TEST VOLTAGE (0°C to 50°C)	FULL SCALE VOLTAGE (0°C to 50°C)	
				Up to 3.2 MΩ	Up to 32 MΩ
Ω	500V dc 500V ac rms (sine)	<1s (up to 320 kΩ) <2s (up to 3.2 MΩ) <10s (up to 32 MΩ)	<3.1V dc (<2.8V dc typical)	<440 mV dc (<420 mV dc typical)	<1.4V dc (<1.3V dc typical)

	MAXIMUM OVERLOAD (across input terminals)	TEST CURRENT	
		Test Current (typical)	V_F
⊣◆))))]	500V dc 500V ac rms (sine)	0.7 mA 0.5 mA 0.3 mA 0.1 mA	0.0V 0.6V 1.2V 2.0V

Basic electrical specifications are defined over the temperature range from 18°C to 28°C for a period of one year after calibration.

Accuracy is specified as ±([% of reading] + [number of units in least significant digit]). In Touch Hold, accuracy is not specified for 300mV⎓ and Ω functions when test circuit impedance exceeds 1 MΩ.

V~ and A~ are average responding, calibrated for the rms value of sine waves.

Useful frequency response (typical): for 32V and 320V ranges, -0.5 dB at 10 kHz; for 3.2V and 750V ranges, ±3 dB at 5 kHz.

Figure A3: Specifications of Fluke 77 multimeter.

APPENDIX B

CALIBRATION MEASUREMENTS RESULTS

In this appendix the results of calibration measurements as described in par. 4.4 can be found.

Measurement series no. 1

T_{real} [K]	0.92 B_{λ_1,λ_2} [W m^{-2} sr^{-1}]	P_{λ_1,λ_2} [W]	E_{λ_1,λ_2} [V]	C [V/W]
1387	$1.35 \cdot 10^{2}$	$6.71 \cdot 10^{-8}$	0.007	$1.04 \cdot 10^{5}$
1437	$2.05 \cdot 10^{2}$	$1.02 \cdot 10^{-7}$	0.011	$1.08 \cdot 10^{5}$
1487	$3.02 \cdot 10^{2}$	$1.50 \cdot 10^{-7}$	0.017	$1.13 \cdot 10^{5}$
1538	$4.39 \cdot 10^{2}$	$2.18 \cdot 10^{-7}$	0.024	$1.10 \cdot 10^{5}$
1588	$6.04 \cdot 10^{2}$	$3.00 \cdot 10^{-7}$	0.034	$1.13 \cdot 10^{5}$
1688	$1.13 \cdot 10^{3}$	$5.62 \cdot 10^{-7}$	0.063	$1.12 \cdot 10^{5}$
1788	$2.03 \cdot 10^{3}$	$1.01 \cdot 10^{-6}$	0.112	$1.11 \cdot 10^{5}$
1887	$3.39 \cdot 10^{3}$	$1.69 \cdot 10^{-6}$	0.186	$1.10 \cdot 10^{5}$
1987	$5.43 \cdot 10^{3}$	$2.70 \cdot 10^{-6}$	0.292	$1.08 \cdot 10^{5}$
2086	$8.35 \cdot 10^{3}$	$4.15 \cdot 10^{-6}$	0.438	$1.05 \cdot 10^{5}$
2186	$1.24 \cdot 10^{4}$	$6.17 \cdot 10^{-6}$	0.634	$1.03 \cdot 10^{5}$
2285	$1.78 \cdot 10^{4}$	$8.85 \cdot 10^{-6}$	0.899	$1.02 \cdot 10^{5}$
2385	$2.48 \cdot 10^{4}$	$1.23 \cdot 10^{-5}$	1.247	$1.01 \cdot 10^{5}$
2484	$3.40 \cdot 10^{4}$	$1.69 \cdot 10^{-5}$	1.721	$1.02 \cdot 10^{5}$
2584	$4.55 \cdot 10^{4}$	$2.26 \cdot 10^{-5}$	2.291	$1.01 \cdot 10^{5}$

$A_1 = 607 \cdot 10^{-6}$ m^2

$r_c = 2.3745$ m

$A_s = 4.62 \cdot 10^{-6}$ m^2

$$C = \frac{E_{\lambda_1,\lambda_2}}{P_{\lambda_1,\lambda_2}} = \frac{E_{\lambda_1,\lambda_2} \cdot r_c^2}{B_{\lambda_1,\lambda_2} \cdot A_1 \cdot A_s}$$

Measurement series no. 2

T_{real} [K]	0.92 B_{λ_1,λ_2} [W m^{-2} sr^{-1}]	P_{λ_1,λ_2} [W]	E_{λ_1,λ_2} [V]	C [V/W]
1387	$1.35 \cdot 10^{2}$	$4.77 \cdot 10^{-8}$	0.006	$1.26 \cdot 10^{5}$
1437	$2.05 \cdot 10^{2}$	$7.24 \cdot 10^{-8}$	0.009	$1.24 \cdot 10^{5}$
1487	$3.02 \cdot 10^{2}$	$1.07 \cdot 10^{-8}$	0.012	$1.13 \cdot 10^{5}$
1538	$4.39 \cdot 10^{2}$	$1.55 \cdot 10^{-7}$	0.017	$1.10 \cdot 10^{5}$
1588	$6.04 \cdot 10^{2}$	$2.13 \cdot 10^{-7}$	0.025	$1.17 \cdot 10^{5}$
1688	$1.13 \cdot 10^{3}$	$3.99 \cdot 10^{-7}$	0.046	$1.15 \cdot 10^{5}$
1788	$2.03 \cdot 10^{3}$	$7.17 \cdot 10^{-7}$	0.080	$1.12 \cdot 10^{5}$
1887	$3.39 \cdot 10^{3}$	$1.20 \cdot 10^{-6}$	0.131	$1.09 \cdot 10^{5}$
1987	$5.43 \cdot 10^{3}$	$1.92 \cdot 10^{-6}$	0.206	$1.07 \cdot 10^{5}$
2086	$8.35 \cdot 10^{3}$	$2.95 \cdot 10^{-6}$	0.308	$1.04 \cdot 10^{5}$
2186	$1.24 \cdot 10^{4}$	$4.38 \cdot 10^{-6}$	0.446	$1.02 \cdot 10^{5}$
2285	$1.78 \cdot 10^{4}$	$6.29 \cdot 10^{-6}$	0.632	$1.01 \cdot 10^{5}$
2385	$2.48 \cdot 10^{4}$	$8.76 \cdot 10^{-6}$	0.876	$1.00 \cdot 10^{5}$
2384	$3.40 \cdot 10^{4}$	$1.20 \cdot 10^{-5}$	1.210	$1.01 \cdot 10^{5}$
2584	$4.55 \cdot 10^{4}$	$1.61 \cdot 10^{-5}$	1.610	$1.00 \cdot 10^{5}$

$A_1 = 431 \cdot 10^{-6}$ m^2

$A_s = 4.62 \cdot 10^{-6}$ m^2

$r_c = 2.3745$ m

Measurement series no. 3

T_{real} [K]	0.92 B_{λ_1,λ_2} [W m^{-2} sr^{-1}]	P_{λ_1,λ_2} [W]	E_{λ_1,λ_2} [V]	C [V/W]
1387	$1.35 \cdot 10^{2}$	$3.66 \cdot 10^{-7}$	0.048	$1.31 \cdot 10^{5}$
1437	$2.05 \cdot 10^{2}$	$5.56 \cdot 10^{-7}$	0.069	$1.24 \cdot 10^{5}$
1487	$3.02 \cdot 10^{2}$	$8.19 \cdot 10^{-7}$	0.101	$1.23 \cdot 10^{5}$
1538	$4.39 \cdot 10^{2}$	$1.19 \cdot 10^{-6}$	0.141	$1.18 \cdot 10^{5}$
1588	$6.04 \cdot 10^{2}$	$1.64 \cdot 10^{-6}$	0.199	$1.21 \cdot 10^{5}$
1688	$1.13 \cdot 10^{3}$	$3.07 \cdot 10^{-6}$	0.364	$1.19 \cdot 10^{5}$
1788	$2.03 \cdot 10^{3}$	$5.51 \cdot 10^{-6}$	0.633	$1.15 \cdot 10^{5}$
1887	$3.39 \cdot 10^{3}$	$9.20 \cdot 10^{-6}$	1.047	$1.14 \cdot 10^{5}$
1987	$5.43 \cdot 10^{3}$	$1.47 \cdot 10^{-5}$	1.636	$1.11 \cdot 10^{5}$
2086	$8.35 \cdot 10^{3}$	$2.26 \cdot 10^{-5}$	2.445	$1.08 \cdot 10^{5}$
2186	$1.24 \cdot 10^{4}$	$3.36 \cdot 10^{-5}$	3.54	$1.05 \cdot 10^{5}$
2285	$1.78 \cdot 10^{4}$	$4.83 \cdot 10^{-5}$	5.01	$1.04 \cdot 10^{5}$
2385	$2.48 \cdot 10^{4}$	$6.73 \cdot 10^{-5}$	6.93	$1.03 \cdot 10^{5}$
2384	$3.40 \cdot 10^{4}$	$9.22 \cdot 10^{-5}$	9.45	$1.02 \cdot 10^{5}$
2584*	$4.55 \cdot 10^{4}$	$1.23 \cdot 10^{-4}$	12.20	$9.88 \cdot 10^{4}$

$A_1 = 607 \cdot 10^{-6}$ m^2

$A_s = 4.88 \cdot 10^{-6}$ m^2

$r_c = 1.045$ m

* measurement not taken into account

Measurement series no. 4

T_{real} [K]	0.92 B_{λ_1,λ_2} [$Wm^{-2}\ sr^{-1}$]	P_{λ_1,λ_2} [W]	E_{λ_1,λ_2} [V]	C [V/W]
1387	$1.35 \cdot 10^{2}$	$2.30 \cdot 10^{-7}$	0.028	$1.22 \cdot 10^{5}$
1437	$2.05 \cdot 10^{2}$	$3.50 \cdot 10^{-7}$	0.042	$1.20 \cdot 10^{5}$
1487	$3.02 \cdot 10^{2}$	$5.15 \cdot 10^{-7}$	0.062	$1.20 \cdot 10^{5}$
1538	$4.39 \cdot 10^{2}$	$7.49 \cdot 10^{-7}$	0.088	$1.18 \cdot 10^{5}$
1588	$6.04 \cdot 10^{2}$	$1.03 \cdot 10^{-6}$	0.124	$1.20 \cdot 10^{5}$
1688	$1.13 \cdot 10^{3}$	$1.93 \cdot 10^{-6}$	0.225	$1.17 \cdot 10^{5}$
1788	$2.03 \cdot 10^{3}$	$3.46 \cdot 10^{-6}$	0.395	$1.14 \cdot 10^{5}$
1887	$3.39 \cdot 10^{3}$	$5.78 \cdot 10^{-6}$	0.652	$1.13 \cdot 10^{5}$
1987	$5.43 \cdot 10^{3}$	$9.26 \cdot 10^{-6}$	1.029	$1.11 \cdot 10^{5}$
2086	$8.35 \cdot 10^{3}$	$1.42 \cdot 10^{-5}$	1.539	$1.08 \cdot 10^{5}$
2186	$1.24 \cdot 10^{4}$	$2.11 \cdot 10^{-5}$	2.227	$1.05 \cdot 10^{5}$
2285	$1.78 \cdot 10^{4}$	$3.04 \cdot 10^{-5}$	3.156	$1.04 \cdot 10^{5}$
2385	$2.48 \cdot 10^{4}$	$4.23 \cdot 10^{-5}$	4.38	$1.04 \cdot 10^{5}$
2484	$3.40 \cdot 10^{4}$	$5.80 \cdot 10^{-5}$	6.05	$1.04 \cdot 10^{5}$
2584	$4.55 \cdot 10^{4}$	$7.75 \cdot 10^{-5}$	8.09	$1.04 \cdot 10^{5}$

$A_1 = 607 \cdot 10^{-6}\ m^2$

$A_s = 4.77 \cdot 10^{-6}\ m^2$

$r_c = 1.303\ m$

APPENDIX C

HANDLEIDING VOOR DE BEDIENING VAN DE STRALINGSMETER

P.J.M. Elands
Rijswijk, september 1985

Inhoud

1. Apparatuur

De te gebruiken apparatuur bestaat uit de volgende attributen (fig. 1):
(1) de Hasselblad-camera met daarin gemonteerd een diode, die op zijn beurt, via een BNC-kabel is verbonden met (2) een versterker. Verder wordt gebruik gemaakt van een diafragma en schermen (3).

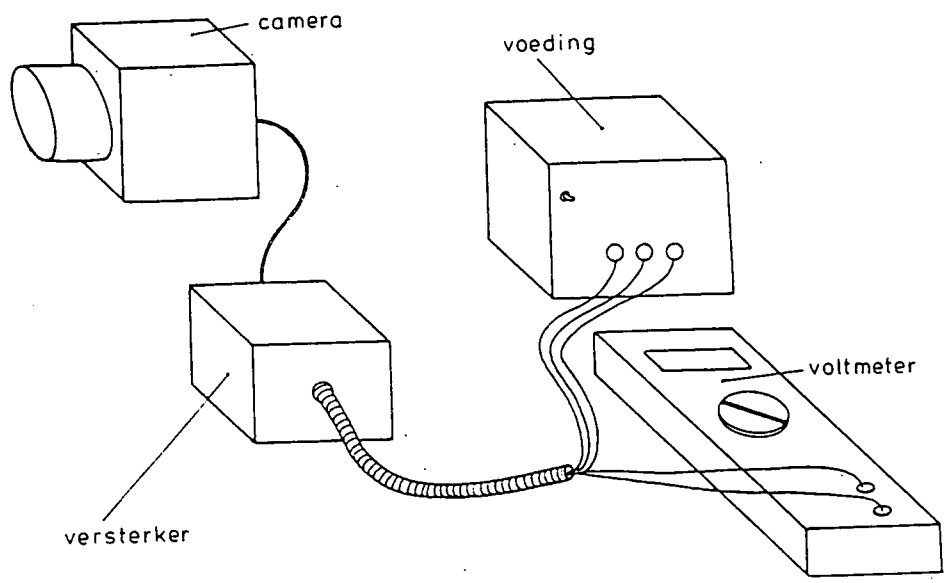

Figuur 1: Te gebruiken apparatuur.

1.1. De camera met diode

De camera bezit een lens waarvan de effectieve diameter geregeld wordt met een diafragma. De ingestelde diameter kan worden afgelezen op de lensvatting. Het getal 2.8, de maximale opening, geeft aan brandpuntsafstand gedeeld door diameter. Hoe groter het geselecteerde diafragmagetal, hoe kleiner dus de diameter en hoe kleiner dus de opgenomen hoeveelheid licht.
We werken steeds met een zo groot mogelijke diameter, dus zo klein mogelijk diafragmagetal, echter met inachtname van par. 5.
Het centrum van de cameralens, ten opzichte waarvoor afstanden moeten worden gemeten, bevindt zich 43 mm achter de voorkant van het lensmontuur (deze voorkant is een bajonetvatting). De camera bezit een sluiter, die, voor ons gebruik,

of steeds licht doorlaat of steeds licht tegenhoudt, en daarom ingesteld staat op 'B'.
De sluiter wordt bediend met de sluiterknop, deze moet voor ons gebruik op 'T' ingesteld staan.
Op de plaats waar zich normaal de film bevindt, is de lichtgevoelige diode gemonteerd, in de uitneembare achterwand van de camera.
Belangrijk: Raak deze diode nooit aan! Eventuele beschadiging en noodzaak tot herijking zijn het gevolg.

1.2. De versterker

Uit de versterker komen 5 draden, die volgens onderstaande tabel moeten worden aangesloten:

draad	stekker	plaats/funktie
blauw	groen	voeding -15 V
geel/groen	geel	voeding +15 V
zwart	zwart	voeding 0 V
lichtbruin	wit	uitgangsspanning 0 V
donkerbruin	rood	uitgangsspanning E

Tabel 1: aansluitpunten versterkerdraden.

De uitgangsspanning wordt gemeten met behulp van een voltmeter of wordt rechtstreeks aangesloten op het data-acquisitiesysteem.
De versterker is op een bepaalde versterking ingesteld. Met deze versterking is de gehele stralingsmeter geijkt. Deze versterking mag dus niet (zonder meer) veranderd worden. Is dit per ongeluk toch gebeurd, dan moet aan de hand van par. 7 de juiste versterking opnieuw worden ingesteld. Zie hiervoor ook het rapport 'Visible radiation measurement for temperature determination'.

1.3. Het diafragma en de tussenschermen

Het zwarte diafragma bestaat uit een scherm waarin één van een aantal verschillende insteek-openingen is gestoken. Deze openingen met welbekende maten, definiëren het stralend oppervlak waaraan wordt gemeten. Het scherm van het diafragma heeft zijwanden die op het scherm vallend licht, op en nabij de insteekopeningen, voorkomen.

De zwarte tussenschermen schermen strooilicht van buiten het diafragma af. Ze zijn daartoe eveneens voorzien van zijwanden. Achter de VBVK dient een zwart afsluitscherm aanwezig te zijn om meetbaar doorvallend licht tegen te houden.

2. Positionering van camera, diafragma en tussenschermen

1. Bepaal de grootte en de plaats van het te meten stralend oppervlak.
2. Plaats de camera voor de VBVK zo dat de optische as van de camera de hartlijn van de cilinder loodrecht doorsnijdt op de plaats van het te meten oppervlak. Voor de afstand camera-VBVK, zie verderop onder opmerking 2.
3. Het te meten oppervlak wordt geselecteerd door het diafragma met de juiste insteekopening zo dicht mogelijk bij de VBVK te plaatsen. Let erop dat, gezien vanuit de camera, de gehele insteekopening zo homogeen mogelijk gevuld zal zijn met licht van de VBVK.
4. Buiten het voorzetdiafragma dient het zo donker mogelijk te zijn. Dit wordt onder andere bereikt met het zo goed mogelijk plaatsen van de tussenschermen.
5. Plaats het afsluitscherm zodanig dat geen storende reflecties hieraan optreden.

   De camera, het diafragma en de tussenschermen dienen natuurlijk zo opgesteld te worden dat iedere verbindingslijn tussen een punt van het stralend oppervlak en een punt van de lensopening niet onderbroken wordt. Ter controle kan met een spiegeltje bekeken worden of vanuit ieder punt van de lens ook de gehele insteekopening zichtbaar is.

Opmerkingen:

1. De verlichting van de proefruimte dient zo veel mogelijk beperkt te worden.
2. De afstand tussen de stralingsbron en de lens is per definitie de afstand tussen voorzetdiafragma en voorzijde van lensmontuur +43 mm, zie figuur 2. De grootte van deze afstand is 10 à 50 cm per cm^2 voorzetdiafragmaopening. Het is aan te bevelen deze afstand, alsmede de afstand VBVK-voortzetdiafragma zoveel mogelijk standaard te kiezen.

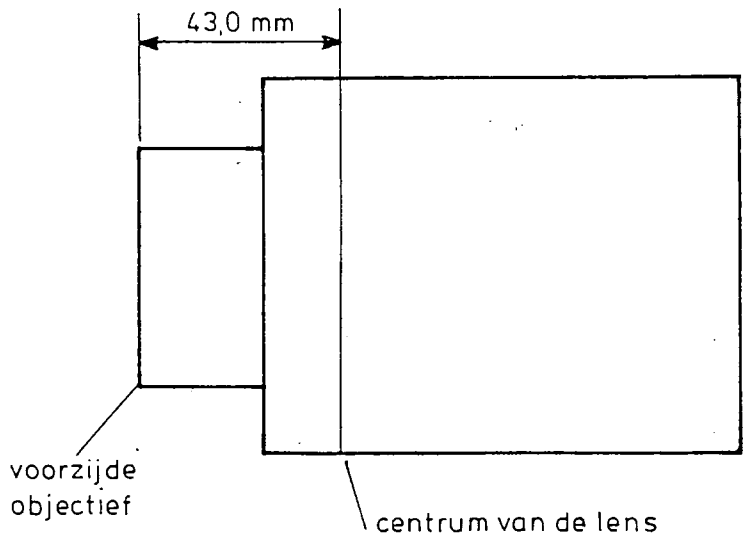

Figuur 2: Afstand tussen voorzijde objectief en lens.

3. Camera-instelling

De afstandsinstelling: scherp instellen op insteekopening bij de VBVK.
De sluitertijdinstelling: B.
Diafragma-instelling: openingsdiameter zo groot mogelijk, dus zo klein mogelijk nummer, echter met inachtneming van par. 5.
De oppervlakten van de lensopeningen staan vermeld in het SFCC-rapport 'Visible radiation measurement for temperature determination'.

De volgorde van instellen van de camera luidt:
1. diafragma kiezen;
2. spannen met behulp van draaiknop;
3. ontspanknop rechtsonder op positie 'T' zetten;
4. afdrukken, sluiter blijft open. De camera is nu meetklaar.

Na afloop de ontspanknop op positie '0' zetten; de sluiter klapt dicht.

4. VBVK

Het manteloppervlak van de plexiglas cilinder dient blinkend schoon gepoetst te zijn, glad en zonder krassen. Verontreiniging door vingerafdrukken geeft tot ca 10% vermindering in straling.

5. Meting

Begin met een achtergrondlichtmeting dus onder proefomstandigheden, echter zonder VBVK. Doe aan het eind van de VBVK-metingen indien mogelijk nog een achtergrondmeting. Het gemiddelde achtergrondlicht van de meetresultaten aftrekken.
Het uitgangssignaal dient bij voorkeur beneden de 7 V te blijven! Hoger dan 10 V is geheel onbetrouwbaar. Tussen de 7 en 10 V is de verzadiging significant maar bekend, zie de verzadigingskromme (fig. 3.4 in het SFCC-rapport).
Bij gering uitgangssignaal is de invloed van ruis en storingen relatief groot. Probeer zo te werk te gaan met het instellen van de voorzetdiafragma-opening en van de afstand tussen voorzetdiafragma en camera dat bij $\Delta = 2.8$ het uitgangssignaal tussen 1 V en 7 V ligt.

6. Meetresultaten

Bij een serie metingen dienen de volgende grootheden genoteerd te worden (inclusief fouten):
- diafragmanummer Δ,
- oppervlakte van het voorzetdiafragma A_s,
- afstand r (voorzetdiafragma tot voorzijde objectief +43,0 mm),
- uitgangsspanning $E_{\lambda_1,\lambda_2}(t)$ (ev. uit data-acquisitiesysteem),
- achtergrondlichtsignaal E_{BG}.

7. IJking versterker en diode

De versterking kan worden gecontroleerd door op de open zijde van de 825 kΩ weerstand R_c (zie het versterkerschema figuur 3) een spanning van 3.000 V aan te brengen.

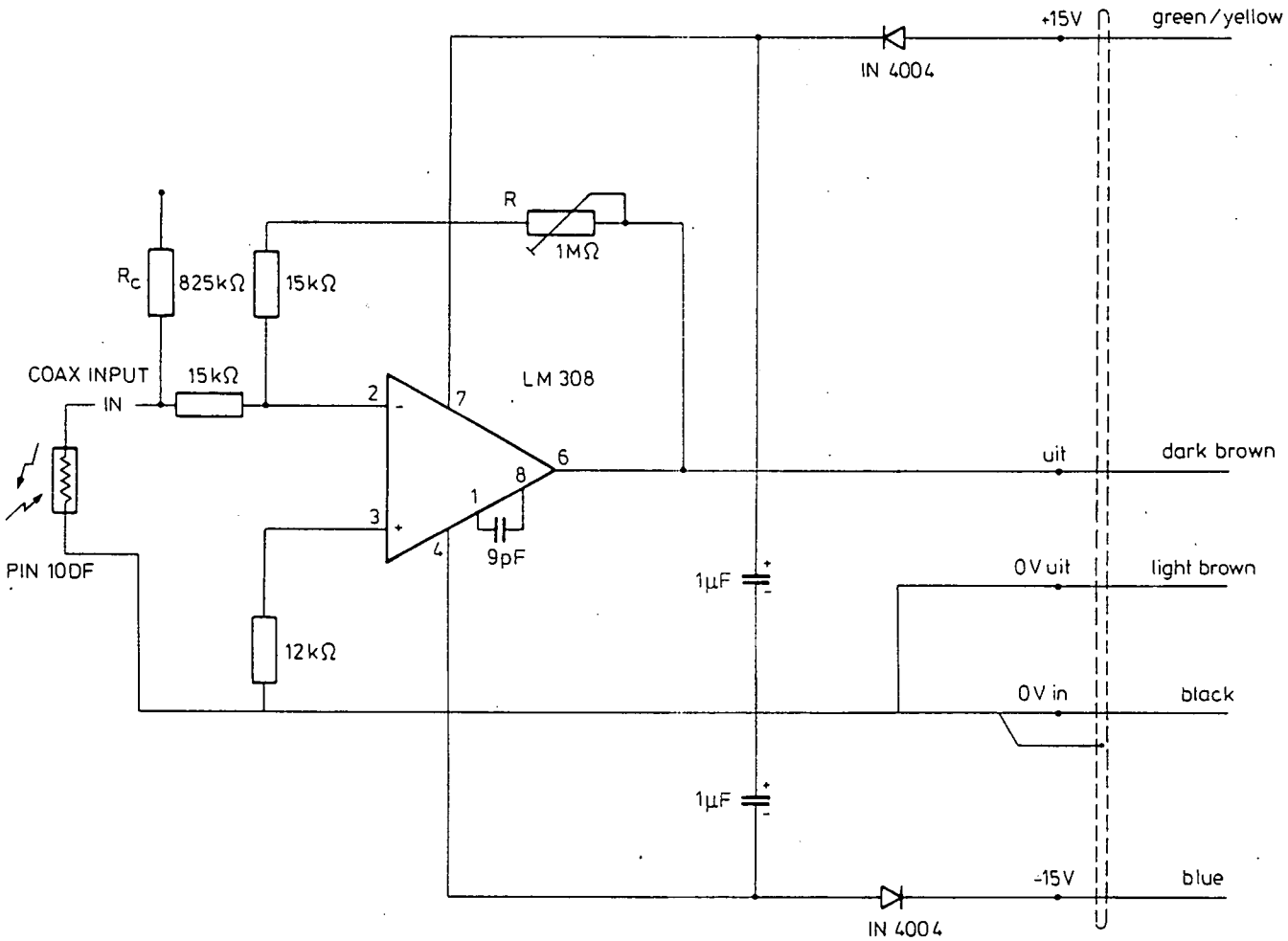

Figuur 3: Amplifier.

Bij de juiste versterking bedraagt de uitgangsspanning 2.431 V. Is dit niet het geval dan moet de regelbare weerstand alsnog zodanig ingesteld worden, tot bij bovengenoemde ijkspanning dezelfde uitgangsspaning wordt gemeten.
Indien uit de praktijk blijkt dat de versterking van de versterker een te sterk of te zwak signaal geeft, dan kan deze versterking gewijzigd worden mits de nieuwe verhouding tussen ijkspanning (op de 825 kΩ weerstand) en de uitgangsspanning nauwkeurig wordt gemeten en opgetekend. De verandering in versterking dient dan in de calibratie of in de berekening van de radiantie B en de temperatuur T verwerkt te worden.

De diode heeft de juiste respons wanneer de uitgangsspanning bij het plaatsen van het ijkbuisje met de LEDjes overeenkomt met de waarde uit het laatste ijkrapport.

8. Verwijzing

Beschrijving van de methode en van de calibratie is te vinden in de SFCC-publikatie 'Visible Radiation Measurement for Temperature Determination'.